Ore Geology Reviews 86 (2017) 196–211

Contents lists available at ScienceDirect

Ore Geology Reviews

journal homepage: www.elsevier.com/locate/oregeo

Geochronological framework of the Xiadian gold deposit in the Jiaodong province, China: Implications for the timing of gold mineralization

Wei-Dong Ma [a,b], Hong-Rui Fan [a,b,*], Xuan Liu [a], Franco Pirajno [c], Fang-Fang Hu [a,b], Kui-Feng Yang [a,b], Yue-Heng Yang [d], Wen-Gang Xu [a], Peng Jiang [a,b]

[a] Key Laboratory of Mineral Resources, Institute of Geology and Geophysics, Chinese Academy of Sciences, Beijing 100029, China
[b] College of Earth Science, University of Chinese Academy of Sciences, Beijing 100049, China
[c] Centre for Exploration Targeting, University of Western Australia, Crawley, WA 6009, Australia
[d] State Key Laboratory of Lithospheric Evolution, Institute of Geology and Geophysics, Chinese Academy of Sciences, Beijing 100029, China

ARTICLE INFO

Article history:
Received 18 June 2016
Available online 16 February 2017

Keywords:
Monazite U–Pb geochronology
Molybdenite Re–Os dating
Linglong granite
Guojialing granodiorite
Xiadian gold deposit
Jiaodong

ABSTRACT

The Xiadian gold deposit, located in the Zhaoyuan–Laizhou belt of the Jiaodong gold province, is a typical Jiaojia-type gold deposit, which is characterized by disseminated and stockwork ores enclosed by hydrothermally altered wall rocks. The exact age and the genesis of the gold deposit remain controversial. Here, we present precise in-situ monazite U-Pb dating to constrain the age of the gold mineralization, which we integrate with published geochronological work on the associated geological events to understand the genesis of the gold deposit. The Linglong granite represents the earliest magmatic event at Xiadian, and yielded a zircon LA–ICPMS U-Pb age of 159.5 ± 0.9 Ma (2σ, MSWD = 0.63). Subsequent geologic events were recorded by minor amounts of quartz–pyrite–molybdenite veins which are dated at 124.8 ± 2.1 Ma (2σ, MSWD = 0.01) by molybdenite Re–Os dating in a granitic pegmatite. The formation of such veins was close to the emplacement of adjacent Guojialing granodiorite (~130 Ma), and thus may be considered as a product of post–magmatic hydrothermal activity. It is proposed that the molybdenum–bearing hydrothermal fluids acted as a prelude to gold mineralization and participated in the formation of the latter ore fluids. Gold mineralization took place at 120.0 ± 1.4 Ma (2σ, MSWD = 0.59), determined by LA–ICPMS U–Pb dating on hydrothermal monazite from quartz–polymetallic sulfide veins. Prior to and post mineralization, voluminous hydrothermally altered porphyritic diorite and fresh quartz diorite porphyry dykes were emplaced, which yielded U–Pb ages of 121.3 ± 1.4 Ma (2σ, MSWD = 0.28) and 115.8 ± 1.9 Ma (2σ, MSWD = 0.71), respectively. Based on these geochronological data, we have established a comprehensive geochronologic framework, which suggests that the genesis of the Xiadian deposit might be related to the craton destruction and lithosphere thinning in the North China Craton.

1. Introduction

Jiaodong gold province, with an area of approximately 3500 km^2, is located within the southeastern margin of the North China Craton (Fig. 1) and is the largest gold producing region in China with reserves of >3000 t gold (Goldfarb and Santosh, 2014). The Zhaoyuan–Laizhou gold belt, situated in the northwestern Jiaodong province, hosts several giant gold deposits, like Sanshandao, Jiaojia, Xincheng, Linglong, and Dayingezhuang, accounting for over 80% of the Jiaodong gold reserves (Zhou and Lü, 2000). The Xiadian gold deposit, located in the southern part of this belt, is a typical Jiaojia–type gold deposit which is characterized by disseminated and stockwork–style pyrite–sericite–quartz alteration and related ores controlled by the Zhaoyuan–Pingdu fault (Deng et al., 2009; Tan et al., 2012; Yang et al., 2016).

A good knowledge of the timing of mineralization is important to constrain ore genesis and regional metallogeny (Taylor et al., 2015; Yang et al., 2014). Direct dating of hydrothermal gold mineralization is difficult due to the scarcity of both suitable chronometers and in-situ techniques with sufficient spatial resolution and precision (Rasmussen et al., 2006). Attempts to date mineralization events using hydrothermal minerals may result in ambiguous, mixed ages due to the mixing of minerals from different sources and incomplete resetting of the applied isotopic systems

* Corresponding author at: Key Laboratory of Mineral Resources, Institute of Geology and Geophysics, Chinese Academy of Sciences, Beijing 100029, China.
E-mail address: fanhr@mail.iggcas.ac.cn (H.-R. Fan).

http://dx.doi.org/10.1016/j.oregeorev.2017.02.016
0169-1368/

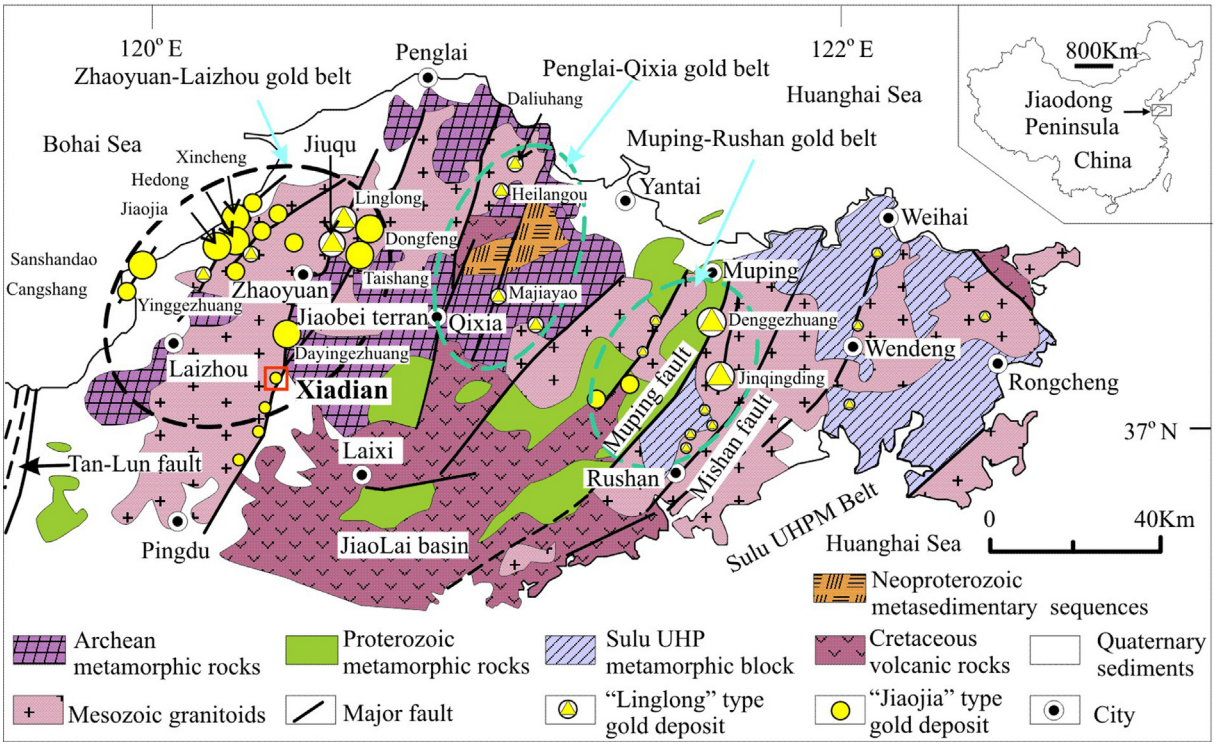

Fig. 1. Simplified geological map of the Jiaodong Peninsula showing location of the major gold deposits (after Fan et al., 2003) The size of the symbols of the gold deposits indicates the gold reserves: large symbol Au>50t, small symbol Au < 50t. Xiadian gold deposit occurs at the northwestern part of the gold province.

(Kazimoto et al., 2015). Previous geochronological studies by Rb–Sr, K–Ar and ^{40}Ar–^{39}Ar dating of alteration minerals (Li et al., 2003, 2006), U–Pb dating of hydrothermal zircon (Hu et al., 2004), as well as ^{40}Ar–^{39}Ar and Rb–Sr dating on quartz and pyrite (Li et al., 2008; Yang and Zhou, 2001), indicated that gold mineralization in the Jiaodong gold province is clustered at 120 ± 5 Ma. Although mineralization and alteration types at the Xiadian gold deposit resemble those of other gold deposits in Jiaodong, its mineralization timing has been controversial. Yang et al. (2016) reported zircon fission track (ZFT) ages for the Xiadian gold deposit, and suggested that the timing of mineralization was close to 130 Ma, and that the mineralization was controlled by the Linglong metamorphic core complex. However, the closure temperature of ZFT (240 ± 50 °C) is lower than the temperature of gold mineralization (ranging from 140°C to 380°C, concentrated at 240°C to 300 °C) at Xiadian gold deposit (Xu et al., 2013). In addition, the complex hydrothermal activity would cause a broad range of ZFT ages. So the age of gold mineralization and the associated geological event remain equivocal. Monazite, if present, is an ideal mineral for dating mineralization events (Janots et al., 2014) in that it has a robust isotopic system (U-Th-Pb) with high closure temperatures (700–750 °C, Smith and Giletti, 1997; Suzuki and Adachi, 1994). In-situ U–Pb dating of monazite is capable of eliminating possible mixing of distinct systems. Although it is rare and commonly small in size in the hydrothermal deposits (Janots et al., 2014), we discovered abundant large monazite grains (10–300 μm) in the gold-bearing quartz–polymetallic sulfide veins at Xiadian, which allow us to constrain the timing of mineralization.

A precise geochronological framework plays a key role in the interpretation of isotope ages of different rocks and in understanding the origin of the ore systems and relationships with regional metallogeny. Debate surrounds the genesis of Jiaodong gold deposits, whether the ore-forming fluid originated from metamorphosed basement or an intrusion (Goldfarb et al., 2001, 2007; Nie et al., 2004; Yang et al., 2014). In addition, molybdenite mineralization in the Xiadian gold deposit has not been reported in previous studies. The issue of whether it represents a distinct episode of hydrothermal activity has not been resolved. In this contribution, we present LA–ICPMS zircon U–Pb ages for the Linglong granite, as well as pre–ore and post–ore porphyry dykes. More importantly, we report high-precision monazite U–Pb ages and molybdenite Re–Os ages for hydrothermal fluid alteration events at the Xiadian deposit. Integrating these new radiometric ages with published data, we are able to establish a temporal framework for the deposit and discuss its significance for geodynamic evolution and regional metallogeny in the Jiaodong province.

2. Regional Geology

The Jiaodong district, located in the eastern part of the North China Craton (NCC) is separated from the Luxi Block by the Tan–Lu (Tancheng–Lujiang) Fault (Fig. 1). Basement rocks comprise two terranes, i.e. the Sulu terrane in the south and the Jiaobei terrane in the north, bordered by the Wulian–Qingdao–Yantai suture (Mao et al., 2008; Tan et al., 2012). The Sulu terrane formed by the northward subduction of the Yangtze Block beneath the NCC during the Triassic (Yang et al., 2005; Xie et al., 2013). The ultrahigh-pressure (UHP) metamorphic rocks in the Sulu orogenic belt are mainly composed of the Neoproterozoic granitic gneisses with subordinate coesite–bearing eclogites, schist and quartzite (Huang et al., 2006; Zhang et al., 2012). The main lithological units in the Jiaobei terrane are Precambrian basement sequences that were intruded and covered by voluminous Mesozoic intrusive and volcanic rocks (Zhou and Lü, 2000). Exposed Precambrian basement rocks mainly include the Archean metamorphic rocks (Jiaodong Group), the Paleoproterozoic (Fenzishan and Jingshan Group) and the Neoproterozoic (Penglai Group) metasedimentary sequences (Tang et al., 2008; Zhai et al., 2001), consisting of mafic to felsic volcanic and sedimentary rocks metamorphosed to

amphibolite or granulite facies. Three groups of zircon ages of granitoid rocks at ~2.9 Ga, ~2.7 Ga and ~2.5 Ga were revealed by previous studies, indicating that the Jiaodong peninsula witnessed three main magmatic events (Wu et al., 2013, 2014; Yang and Li, 2008). Two groups of metamorphic zircon ages of 2.52–2.41 Ga and 1.93–1.81 Ga were recognized in the Jiaodong terrane indicating that the Jiaodong peninsula underwent two main metamorphic events (Jahn et al., 2008; Liu et al., 2013).

The Jiaolai basin is a Cretaceous pull-apart basin, which is composed of the middle Early Cretaceous Laiyang Group (sandy conglomerate and carbon-rich shale), the Late Early Cretaceous Qingshan Group (comprising a lower section of trachybasalt, latite and trachyte, and an upper section of rhyolite flows and pyroclastic rocks were formed at 90–124 Ma), and the Late Cretaceous Wangshi Group (sandy conglomerate and siltstone) (e.g., Liu et al., 2009; Tang et al., 2008).

Mesozoic granitoids are widely distributed in the Jiaodong gold province, and have been subdivided into three main age clusters, i.e. Late Triassic, Late Jurassic, and Early Cretaceous. The Late Triassic granitoids including Jiazishan, Chashan and Xingjia plutons are mainly mantle–derived (Gao et al., 2004) and formed during the collision of North China Craton and Yangtze Blocks at ca. 230–205 Ma (Chen et al., 2003; Yang et al., 2007). The Late Jurassic granitoids, including Linglong, Luanjiahe, Kunyushan, Duogushan and Wendeng bodies consist of medium–grained metaluminous to slightly peraluminous biotite granite, granodiorite and monzonite (Tan et al., 2012). SHRIMP and LA–ICPMS zircon U-Pb ages of these granitoids are mainly between 160 and 150 Ma (Wang et al., 1998; Yang et al., 2012). Detailed petrological and geochemical studies indicated that the Linglong suite was derived from partial melting of the crust without significant contribution of mantle components (Ma et al., 2013; Yang et al., 2012). Previous Re–Os dating suggested two generations of molybdenite mineralization in this region: (1) Xingjiashan molybdenum–tungsten deposit (~158 Ma, Ding et al., 2012; Liu et al., 2011) and (2) molybdenite from pegmatite in the Sanshandao gold deposit (150 Ma, Wen et al., 2015b). Considering the close spatial and temporal relationship between the Xingfushan pluton (160–167 Ma defined by zircon U-Pb dating) (Ding et al., 2012; Liu et al., 2011) and the Linglong granite (160–150 Ma defined by zircon U-Pb dating) (Qiu et al., 2002; Wang et al., 1998), these two molybdenite mineralization events are likely to be genetically related to the Late Jurassic magmatic events. The Early Cretaceous granitoids dated from 130 to 105 Ma by the LA-ICPMS zircon U–Pb method (Yang et al., 2012) and represented by Sanshandao, Shangzhuang, Beijie, Congjia, and Guojialing, are mainly granite to granodiorite from west to east in this uplifted part of the peninsula. Petrological and geochemical data indicate that this Guojialing–type suite was formed by the remelting of Archean lower crust with addition of mantle components, as a response to the subduction of the Pacific Plate and asthenospheric upwelling (Yang et al., 2012). A recent titanite study on such a suite (and its bearing dioritic enclaves) shows that both the Archean lower crust and juvenile mafic lower have experienced a remelting process and mixed at a shallower reservoir, indicating the reactivation of Jiaodong lower curst during Early Cretaceous (Jiang et al., 2016). Mafic to felsic dykes are widely developed within the gold districts. These rocks were mostly emplaced at ca. 122–114 Ma and a few at 110–102 Ma (Cai et al., 2013; Yang and Zhou, 2001). Recently, much younger mafic dykes (~95–87 Ma) were identified based on zircon U–Pb ages (Cai et al., 2013).

Previous geochronological studies of alteration minerals and hydrothermal minerals showed that the gold mineralization in the Jiaodong gold province are clustered at 120 ± 5 Ma (Hu et al., 2004; Li et al., 2003, 2006; Li et al., 2008). Most of the large gold mines in the Jiaodong province are located in the widely distributed Linglong and Guojialing granitoids or their contacts with metamorphic basement. Ores mainly occur as auriferous quartz veins or as massive disseminated- and stockwork-style mineralization. K-feldspathization, sericitization and pervasive silicification are the dominant alteration types. Four stages of hydrothermal alteration can be recognized in most of the gold deposits: 1) stage I, quartz–(minor) pyrite; 2) stage II, pyrite–quartz–sericite–gold; 3) stage III, quartz–base metal sulfide minerals; 4) stage IV, quartz–carbonate. The ore-forming materials of the entire sequence of alteration stages are characteristics of mixed sources revealed by sulfur and Sr–Nd isotopic analyses of pyrite and the associated rocks (Goldfarb and Santosh, 2014; Qiu et al., 2002; Song et al., 2015). Fluid inclusion studies suggested that ore-forming fluids in the Jiaodong gold deposits share similar mineralizing temperatures (170–370 °C) and pressures (0.7–3.3 kbar) as well as similar compositions (characterized by H_2O–CO_2–NaCl ± CH_4, Fan et al., 2003; Wen et al., 2015a). Oxygen and hydrogen isotope data indicate that ore fluids are of magmatic origin (Goldfarb and Santosh, 2014; Qiu et al., 2002; Song et al., 2015). Gold deposits at Jiaodong formed in the same mineralizing–geodynamic conditions, and are interpreted to relate to the Mesozoic cratonic destruction (Song et al., 2015; Zhu et al., 2015).

The regional structures mainly trend east, NE–NNE, and NW–NNW, (Fig. 1). The EW–trending set of faults formed by the north–south compression associated with early Mesozoic collision between the North China and Yangtze Blocks are the earliest of Mesozoic structures (Zhang et al., 2006). The NE– to NNE–trending set of faults developed in eastern China as Late Jurassic sinistral faults that transect the Zhaoyuan area and as Early Cretaceous dextral faults that formed pull–apart basins, such as the Jiaolai basin (Fig. 1; Xu et al., 1987; Zhu et al., 2010). These fault systems are the principal ore–controlling structures (Goldfarb et al., 2001; Qiu et al., 2002), including the Sanshandao–Cangshang, Jiaojia–Xincheng, and Zhaoyuan–Pingdu fault zones, from west to east, and hosting nearly 90% of the gold resources in the Jiaodong peninsula. The NW–trending set of faults developed after the main gold mineralization and often cut the NE– to NNE–trending set of faults (Deng et al., 2010).

3. Deposit Geology

The Xiadian gold deposit is situated at the southern section of the Zhaoyuan–Pingdu fault zone and has a reserve of >200 tons of Au (Yang et al., 2016) (Fig. 1). Mineralization is structurally controlled by the southern part of the NE-treading Zhaoyuan–Pingdu fault (Fig. 2). The deposit is mainly hosted in the footwall of the fault, as well as the contacts between Jiaodong Group and Linglong granitoids (Fig. 3), forming five discontinuous lenticular orebodies. The largest one, Lode VII strikes about 040° and dips 45° to southeast, and is >300 m long and 40–70 m wide. The Linglong granite consists of plagioclase, K-feldspar, quartz, and biotite, with accessory titanite, garnet, zircon and apatite (Fig. 4a). Some pre-ore and post-ore dykes are also present. The pre–ore porphyritic diorite dykes mainly comprise plagioclase, amphibole and biotite with rare clinopyroxene; the dykes are cut by quartz–sulfide veins (Fig. 4b) and display quartz and pyrite alteration (Figs. 4c, 5a and 5b). The post–ore quartz diorite porphyry dykes are composed of quartz, plagioclase, amphibole and biotite and are devoid of mineralization and alteration (Figs. 4d and 5c).

Quartz–pyrite–molybdenite veins cut pegmatite in the 39ZK6 borehole at downhole depths between −738 m and −741 m. Pegmatite was hosted in the silicified Linglong granite, whereas no crosscutting relation was observed through the 39ZK6 drill core. The quartz–pyrite–molybdenite veins are commonly 5–8 mm wide and show no crosscutting relationship with the gold-rich orebodies

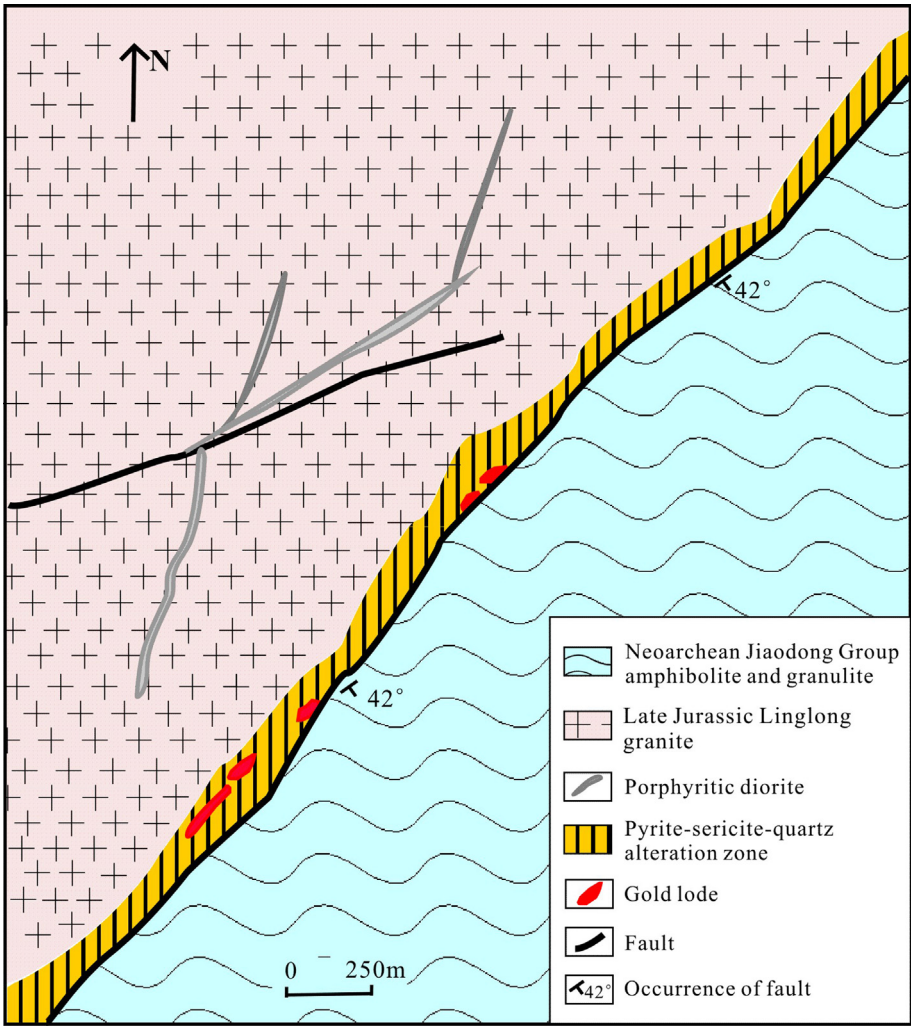

Fig. 2. Simplified regional geological map of the Xiadian gold deposit.

(Fig. 4e). Petrographic and scanning electron microscopy (SEM) observations revealed that molybdenite in the veins is intergrown with pyrite and quartz (Figs. 5d, 6a and 6b). Wall rocks exhibit strong silicification, sericitization, pyrite-sericite-quartz alteration and carbonate alteration. The pyrite–sericite–quartz alteration is accompanied by gold mineralization. Silicification occurred before, during and after gold mineralization. Both the Linglong granitoids and Jiaodong Group display strong strain, locally forming mylonitic rocks (Fig. 3).

Field and optical microscopy investigations indicate four hydrothermal stages at the Xiadian gold deposit, i.e. (I) quartz–pyrite (Figs. 4f, 5e), (II) quartz–sericite–pyrite (Figs. 4g, 5f), (III) quartz–polymetallic sulfide (Figs. 4b, 4h, 5g, 5h, and 5i) and (IV) quartz–calcite–pyrite stages (Fig. 4i). Stage I often appears as quartz–pyrite veins and is characterized by minor white quartz and coarse–grained, euhedral pyrite, and rarely contains Au. Stage II consists of smoky quartz, subhedral pyrite and widespread sericite with minor sphalerite and chalcopyrite presented as quartz–sericite–pyrite bulk ores. Some stage I veins are enclosed in the stage II bulk ores. Stage III comprises large amounts of sulfide minerals, such as pyrite, chalcopyrite, sphalerite, and galena accompanied by abundant electrum and native Au (hereafter referred to as quartz–polymetallic sulfide mineralization). The quartz–polymetallic sulfide veins often cut the above bulk ores and quartz-pyrite veins. Accessory monazite, zircon, apatite, rutile, and thorite (enclosed in monazite) were identified in thin sections. The monazite is typically light yellow in transmitted light, forming euhedral to anhedral crystals of variable size (10–300 μm) (Figs. 5h and 5i). All monazite appear to be compositionally homogeneous under backscattered electrons (BSE) (Fig. 6c–e) conditions. Small monazites are often enclosed by pyrite (Fig. 6c) and quartz. Large monazite grains commonly host pyrite and sericite (Figs. 6d and 6e). Quartz, thorite and rutile are additional mineral inclusions in the monazite. All these features indicate that the monazite was formed during the Stage III hydrothermal mineralization event and associated fluid infiltration into the Linglong granite, resulting in the gold–bearing veins and related minerals. Stage IV is represented by milky carbonate–quartz veins, with trace amounts of pyrite, which crosscut all other vein types.

4. Sampling and analytical methods

4.1. Zircon U–Pb dating

Zircon from Linglong granite, pre–ore and post–ore dykes were selected for U–Pb dating to constrain the age of gold mineralization and the wallrocks in the Xiadian gold deposit. Samples of pre–ore dykes were collected from Line 524 of the −450 m level underground tunnel. Whereas samples of the post–ore dyke were collected from drill hole ZK24 at a depth of −125 m. Unaltered

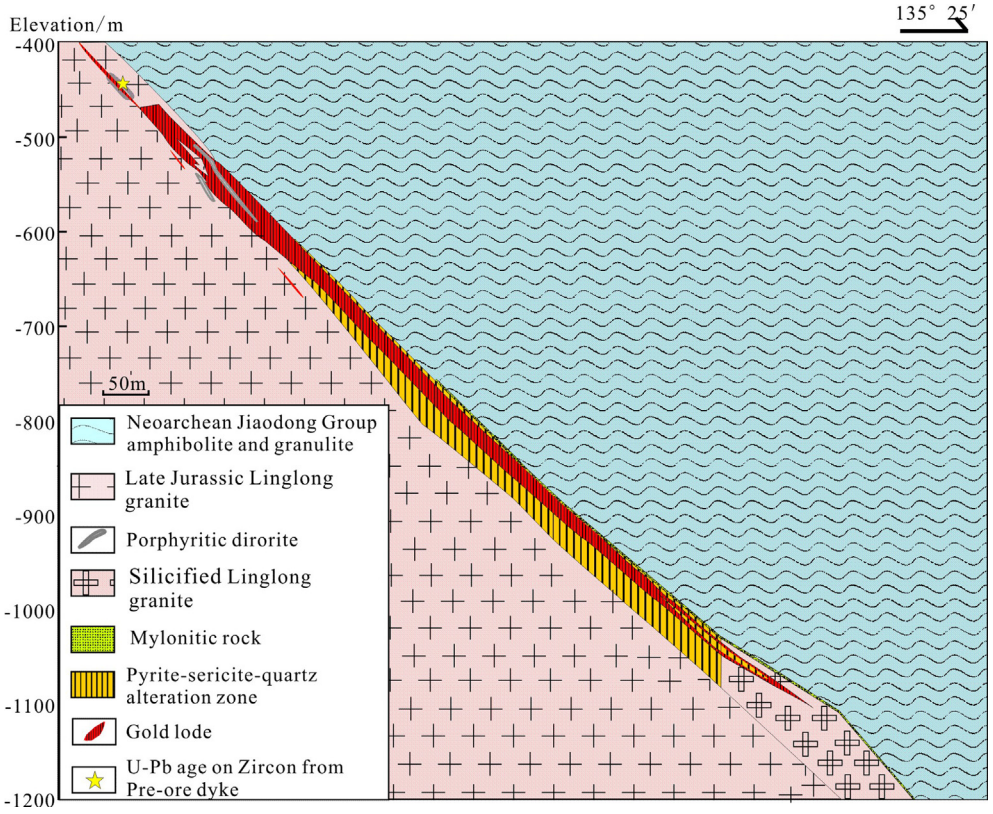

Fig. 3. 524 prospecting line profile of the Xiadian gold deposit.

Linglong granite is not present in the Xiadian gold deposit, thus samples of the Linglong granite from drill hole 116ZK2 at a depth of −1745 m were collected in the adjacent Dayingezhuang gold deposit for constraining the age of the wallrocks of the Xiadian gold deposit.

Zircons were extracted from the whole–rock of the pre-ore dykes (sample 14XD-50), post–ore dykes (sample 24Zk-1-1Y) and Linglong granite (sample 116ZK-2-1745) using standard density and magnetic separation techniques, and then were handpicked under a binocular microscope for purification (purity ≥ 99%) at the Langfang Regional Geological Survey, Hebei Province, China. The selected zircons were mounted in epoxy and polished. Reflected and transmitted light images were obtained by optical microscopy, whereas cathodoluminescence (CL) images were taken by a LEO 1450 scanning electronic microscope at the Institute of Geology and Geophysics, Chinese Academy of Sciences (IGGCAS). The obtained photographs were used to identify internal textures and select target spots for U–Pb dating.

Zircon U–Pb dating was performed by laser ablation ICPMS at the State Key Laboratory of Geological Processes and Mineral Resources, China University of Geosciences, Wuhan, using an Agilent 7500a ICP–MS equipped with a GeoLas 2005 for laser sampling. Detailed operating conditions and data acquisition methods resembled those described by Liu et al. (2010). Each analysis incorporated a background acquisition of approximately 20–30 s (gas blank) followed by 50 s data acquisition from the sample. An Agilent Chemstation was utilized for the acquisition of each individual analysis. Off–line selection and integration of background and analytical signals, time–drift correction, and quantitative calibration for trace element analyses and U–Pb dating were performed by ICPMS Data Cal (Liu et al., 2010).

Zircon 91500 was chosen as the external standard for U–Pb dating and was analyzed twice every five analyses. According to the variations of standard 91500, time–dependent drifts of U–Th–Pb isotopic ratios were corrected using a linear interpolation (with time) for every five analyses (Liu et al., 2010). Preferred U–Th–Pb isotopic ratios used for standard 91500 are sourced from Wiedenbeck et al. (1995). Uncertainties of preferred values for the external standard 91500 were propagated through to the ultimate results of the samples. Isoplot/Ex ver3 was used to make Concordia diagrams and weighted mean calculations (Ludwig, 2012). Representative zircon CL images and analytical results are presented in Fig. 7 and Table 1.

4.2. Molybdenite Re–Os dating

In order to constrain the timing of the molybdenum mineralization, five molybdenite–bearing veinlets were collected for Re–Os dating (14XD-35, 14XD-35-1, 14XD-35-2, 14XD-35-3, 14XD-35-4). Considering the known decoupling effect of the Re–Os molybdenite system (Košler et al., 2003; Selby and Creaser, 2004), our molybdenum samples were crushed to a grain size of about 80 mesh and were then handpicked under a binocular microscope to a purity of ≥99% with samples weighing >30 mg for each sample.

Re–Os isotopic analyses were carried out at the National Research Center of Geoanalysis, Chinese Academy of Geological Sciences, Beijing. The detailed chemical separation procedure follows the description of Du et al. (2004). Accurately weighed 0.2 g aliquots were selected from the sample, loaded into Carius tubes, together with ^{185}Re and ^{190}Os spikes, and digested by reverse aqua regia. Os was separated as OsO_4 by distillation at 105–110 °C and trapped by Milli–Q water. The residue solutions were diluted with distilled water and dried. The solids were then dissolved in a 5 M NaOH solution, from which Re was extracted by acetone.

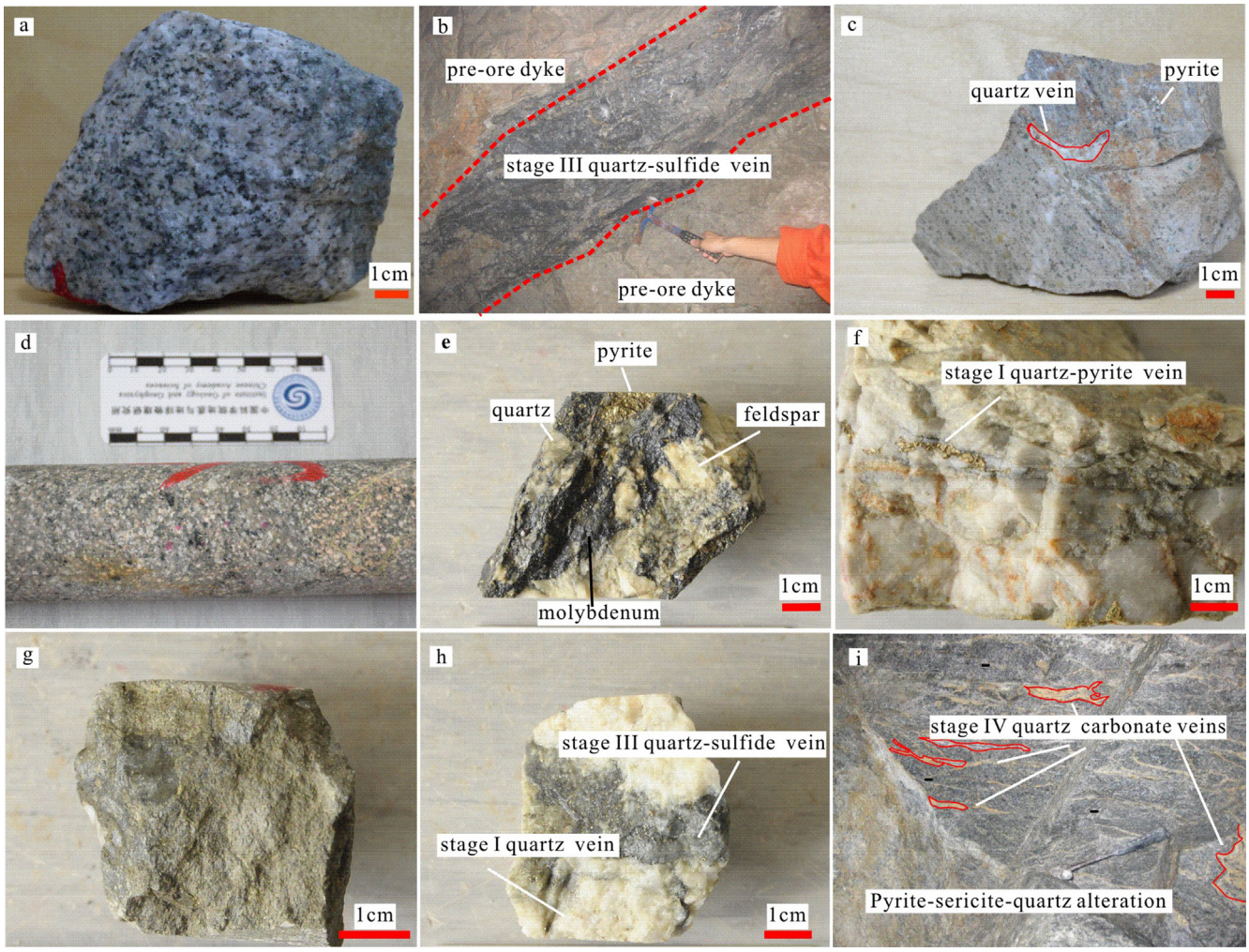

Fig. 4. Photographs showing the ore geology of the Xiadian gold deposit. a, The Linglong granite; b, Middle stage quartz–sulfide vein cut through the pre–ore dyke; c, Pre–ore dyke; d, Unaltered post–ore dyke; e, Quartz–pyrite–molybdenum vein; f, Early stage quartz–sulfide vein; g, Pyrite–sericite–silicate alteration rock; h, Middle stage quartz sulfide vein; i, Quartz–carbonate veins cut through the pyrite–sericite–silicate alteration rock.

Re and Os concentrations and isotopic compositions were determined using a TJA X–series ICPMS. The analytical reliability was tested by analyses of the Certified Reference Material GBW04436 (JDC standard). The Re–Os isochron age was calculated using the least squares method of York (1969), as implemented in the ISOPLOT 3.00 program (Ludwig, 2012). We use $\lambda^{187}Re = 1.666 \times 10^{-11}\ a^{-1}$ as the decay constant in the age calculation determined by Smoliar et al. (1996). Average blanks for the total Carius tube procedure are about 10 pg Re and 0.1 pg Os; ^{187}Os was not detected.

4.3. Monazite U–Pb dating

Quartz–polymetallic sulfide veins that cut the silicified granite in the Xiadian gold deposit at line 518 of the −469 m level underground tunnel were collected for monazite U-Pb dating. The samples were cut into thin sections for subsequent monazite analysis. Reflected and transmitted light images were obtained by optical microscope, whereas BSE images were obtained by a Nova Nano-SEM 450 field emission scanning electronic microscope. The obtained images were used to check for inclusions, cracks, and zoning in the monazite grains. Monazite U–Pb dating was conducted using an Agilent ICPMS, equipped with a Geolas 193 nm excimer laser ablation system. The analytical protocol follows that described by Liu et al. (2012), Sun et al. (2012) and Xie et al. (2008). All the analyses were conducted at the Institute of Geology and Geophysics, Chinese Academy of Sciences.

Monazite U–Pb dating analyses were conducted with a spot size of 35 μm at a repetition rate of 8 Hz. Spot analyses included approximately 20 s of background acquisition and 45 s of sample data acquisition. A matrix–matched external standard (monazite 44069) was used to correct the U/Pb and Th/Pb fractionation and the instrumental mass discrimination utilizing the reference values: $^{207}Pb/^{206}Pb = 0.05532$; $^{207}Pb/^{235}U = 0.06811$; $^{206}Pb/^{238}U = 0.5195$; and $^{208}Pb/^{232}Th = 0.02124$ (Aleinikoff et al., 2006). The Jefferson monazite was measured as an external standard to monitor the accuracy of the analytical procedure. The software package GLITTER 4.0 was used to process the raw U-Pb data. Since the common Pb compositions in our samples are relatively high, the uncorrected compositions of monazite were plotted on a Tera–Wasserburg Concordia diagram (Tera and Wasserburg, 1972). The upper intercept represents the initial $^{207}Pb/^{206}Pb$ ratios, which can be used for common lead correction, and therefore relative precise $^{206}Pb/^{238}U$ ages can be obtained. Both the Tera–Wasserburg Concordia diagram and weighted mean were calculated and plotted by Isoplot/Ex ver3 (Ludwig, 2012). Weighted mean $^{206}Pb/^{238}U$ age of Jefferson monazite (359.7 ± 4.5 Ma (2σ)) and monazite 40669 (422.2 ± 4.4 Ma (2σ)) showed good

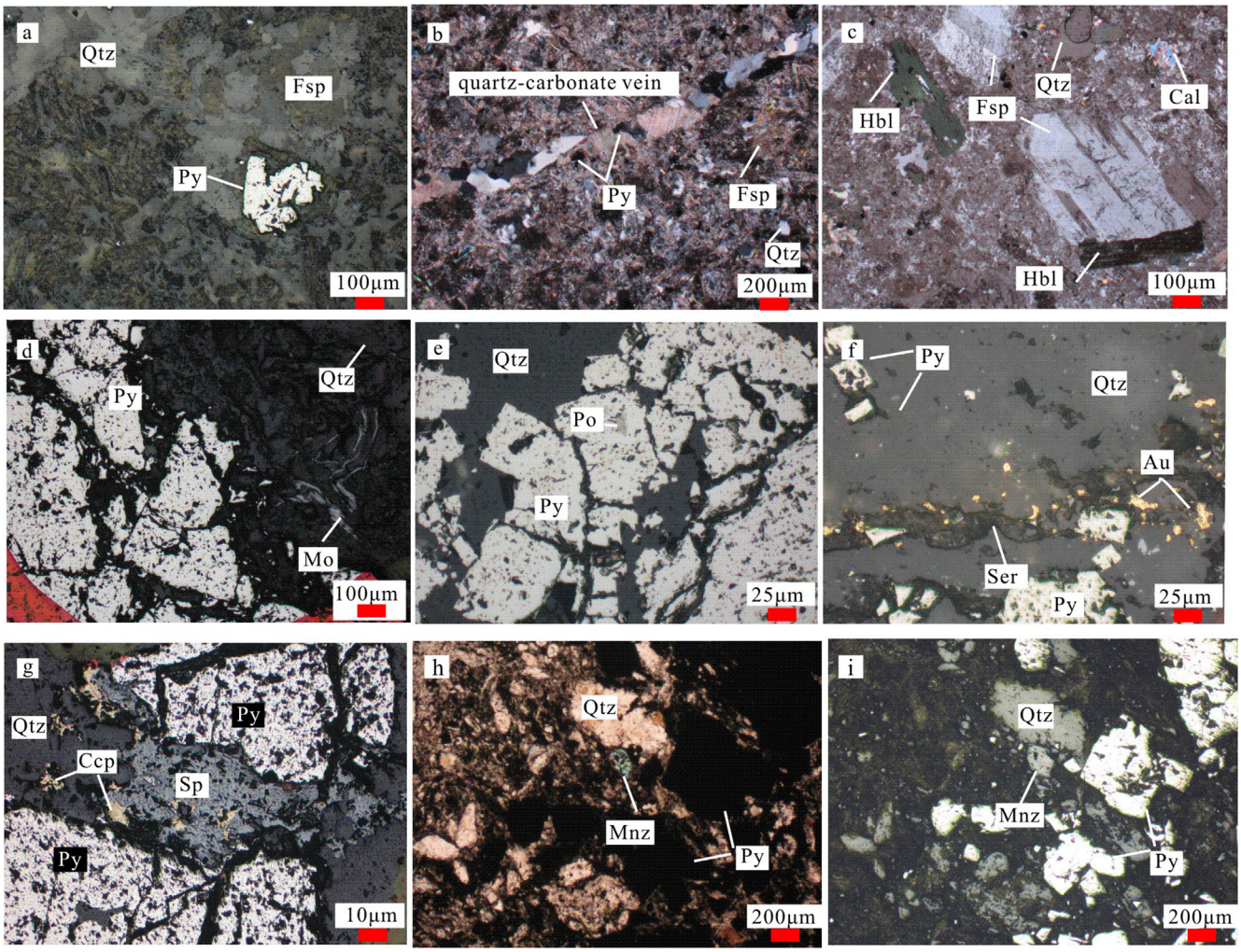

Fig. 5. Photomicrographs under transmitted light (b, c, h), reflected light (a, d–g, i) showing important mineral assemblages. a, Pyrite of the pre–ore dyke; b, Quartz–carbonic vein of the pre–ore dykes, associated with pyrite; c, Quartz, feldspars, hornblende and calcite in the post–ore dyke; d, Pyrite, quartz, molybdenite as disseminated aggregates; e, Quartz, pyrite and pyrrhotite of early quartz–pyrite veins; f, Native gold in sericite, quartz and fractures; g, Typical minerals in quartz–polymetallic sulfide veins, including pyrite, sphalerite, chalcopyrite, galena; h, Monazite in the quartz–polymetallic sulfide veins; i, Monazite in the quartz–polymetallic sulfide veins; Abbreviations: Qtz–quartz, Py–pyrite, Fsp–feldspars, Hbl–hornblende, Mo–molybdenite, Po–pyrrhotite, Ser–sericite, Ccp–chalcopyrite, Sp–sphalerite, Mnz–monazite.

concordance to reported values (within error), i.e. 362.1 ± 3.8 Ma (Alagna et al., 2008) and 424.9 ± 0.5 Ma (Aleinikoff et al., 2006), respectively, which ensure the reliability of our U-Pb results.

5. Analytical results

5.1. Zircon U–Pb dating

Most zircons from the dykes and granite are transparent, colorless to pale brown, and exhibit euhedral, prismatic forms (with length to–width ratios from 2:1 to 3:1). Under cathodoluminescence, zircons commonly show oscillatory zonation except for some dark ones and some with uneven rims (14XD–50 # 3,4,6–9,12–15) which have abnormal ages as detailed below (Fig. 7b).

U-Pb dating results are presented in Table 1. Most of the analytical results plot near the concordia line in Fig. 7d–i. Sixteen spots were analyzed for the Linglong granite, yielding concordant $^{206}Pb/^{238}U$ ages with an upper intercept at ~162 Ma, lower intercept at ~157 Ma and a weighted mean of 159.5 ± 0.9 Ma (2σ, MSWD = 0.63). The weighted $^{206}Pb/^{238}U$ ages are interpreted as the crystallization age of the granite. Fifteen grains were selected from the pre–ore dyke for analysis. Four spots yield concordant $^{206}Pb/^{238}U$ ages with an upper intercept at ~122 Ma, lower intercept at ~120 Ma and weighted mean of 121.3 ± 1.4 Ma (2σ, MSWD = 0.28), representing the age of the intrusion of pre–ore dyke. The other zircon analyses are discordant with $^{206}Pb/^{238}U$ ages ranging from 145.6 ± 13.1 Ma (2σ) to 2080.7 ± 53.2 Ma (2σ) which may not be of magmatic origin as they are dark under CL or with uneven rims. Twenty–one spots were analyzed for post–ore dykes, yielding concordant $^{206}Pb/^{238}U$ ages with an upper intercept at ~120 Ma, lower intercept at ~113 Ma and a weighted mean of 115.8 ± 1.9 Ma (2σ, MSWD = 0.71). The weighted $^{206}Pb/^{238}U$ ages are interpreted as the crystallization age of the zircons and approximate emplacement of the dykes.

5.2. Molybdenite Re–Os age

The Re–Os system in molybdenite is commonly not affected by hydrothermal fluids (Stein et al., 1998) and is resistant to high-temperature fluids (~440 °C) (Selby and Creaser, 2001), so it can provide critical information in unraveling sulfide mineral deposition in ore systems, which may not be recorded by other isotopic systems in alteration minerals. Five molybdenite samples were dated (Table 2). Results show that they have Re contents ranging from 7.8 to 107.1 ppm, and common Os contents from 30 to 50 ppb. On a Re versus Os plot, an optimum isochron age of

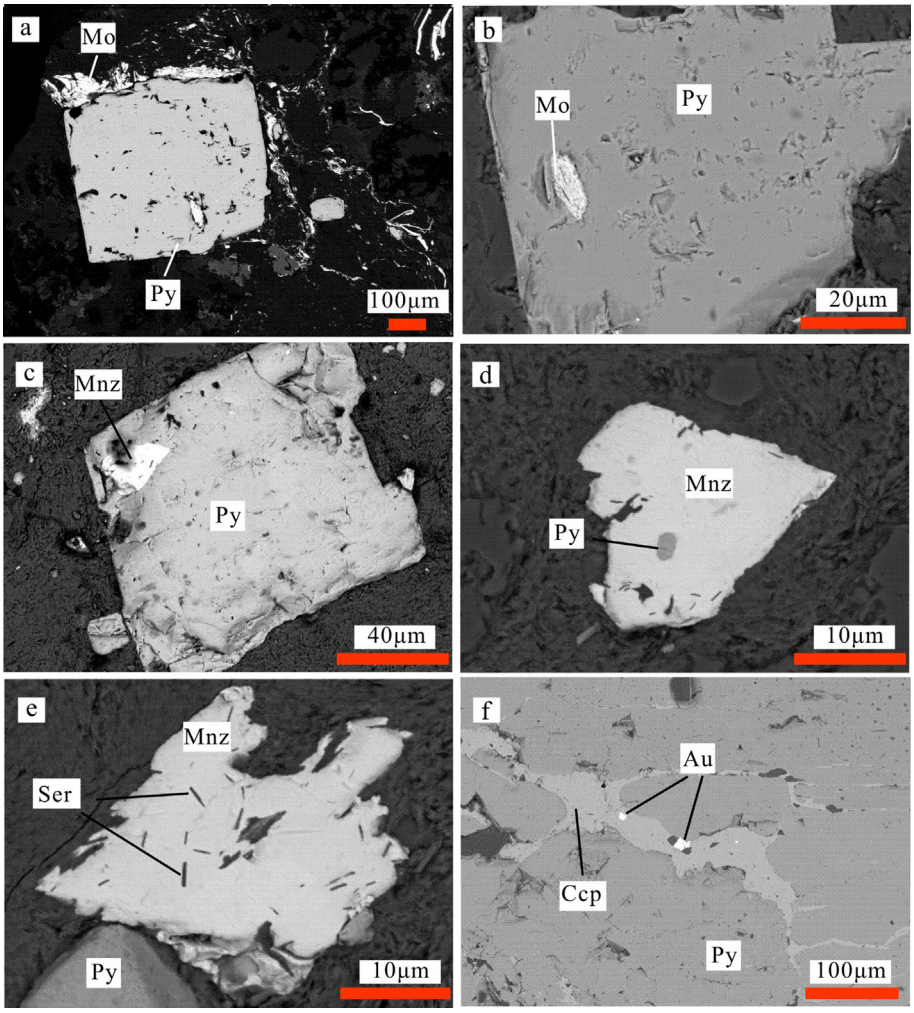

Fig. 6. BSE image showing important mineral assemblages. a, Molybdenite intergrown with pyrite; b, Molybdenite enclosed in the pyrite; c Monazite enclosed in the pyrite; d Pyrite enclosed in the monazite; e Monazite containing sericite; f Quartz–polymetallic sulfide veins containing gold.

124.8 ± 2.1 Ma (2σ, MSWD = 0.10) is obtained (Fig. 8). The model ages range from 125.0 to 126.4 Ma, with a weighted average age of 125.9 ± 0.80 Ma (2σ, MSWD = 0.23).The isochron age is consistent with the weighted average age, reflecting that the molybdenite formed at 125 to 126 Ma.

5.3. Monazite U–Pb dating

The *in-situ* U–Pb dating analyses of twenty-seven spots on monazite grains from two polished thin sections of sample 14XD-111 are presented in Table 3. In contrast to the zircon data, however, the monazite analyses are discordant on a concordia diagram (Fig. 9). The U–Pb data cluster on the Tera–Wasserburg concordia diagram, and give a lower intercept age of 120.2 ± 2.0 Ma (MSWD = 0.78). The initial $^{207}Pb/^{206}Pb$ data is 0.8827 ± 0.02. The ^{207}Pb-corrected weighted $^{206}Pb/^{238}U$ age is 120.0 ± 1.4 Ma (n = 27, MSWD = 0.59) which is in agreement with the lower intercept age.

6. Discussion

6.1. Magmatic and hydrothermal activities affecting the Xiadian gold deposit

The Late Jurassic Linglong granite and Early Cretaceous Guojialing granodiorite, with crystallization ages around 130 Ma, are the main igneous events in the Xiadian gold deposit. Minor molybdenite mineralization represents post-magma hydrothermal activity in this area.

Previous geochronological and geochemical studies implied that the destruction of the North China Craton was initiated in the Late Triassic (Xu and Zhao, 2009; Yang et al., 2009) and the continental extension began as early as 160–150 Ma and was associated with the formation of the continental crust–derived granite (Charles et al., 2013). The obtained LA–ICPMS zircon U–Pb dating of 159.5 ± 0.9 Ma (2σ, MSWD = 0.63) for the Linglong granite in this study agrees well with the previous zircon U–Pb ages of 150 to 160 Ma (Qiu et al., 2002; Wang et al., 1998; Yang et al., 2012). The exposed Linglong granite coincided with the regional Late Jurassic magmatic event (Fig. 10). There are various explanations for the geodynamic mechanism for formation of the Linglong granite (e.g., Jiang et al., 2010; Wu et al., 2005). Geodynamic processes for formation of the Late Jurassic Linglong granite are considered to have been related to large-scale extension of the lithosphere coupled with upwelling of the asthenosphere (Ma et al., 2013; Yang et al., 2012).

During the Early Cretaceous, asthenospheric upwelling caused intense interaction between crust and mantle, with corresponding multi-stage magma mixing and emplacement of the Guojialing granodiorite marking the end the Jiaodong extensional event (Jiang et al., 2016; Mills et al., 2015). Guojialing granodiorite, though not observed in the Xiadian gold deposit, was intercepted

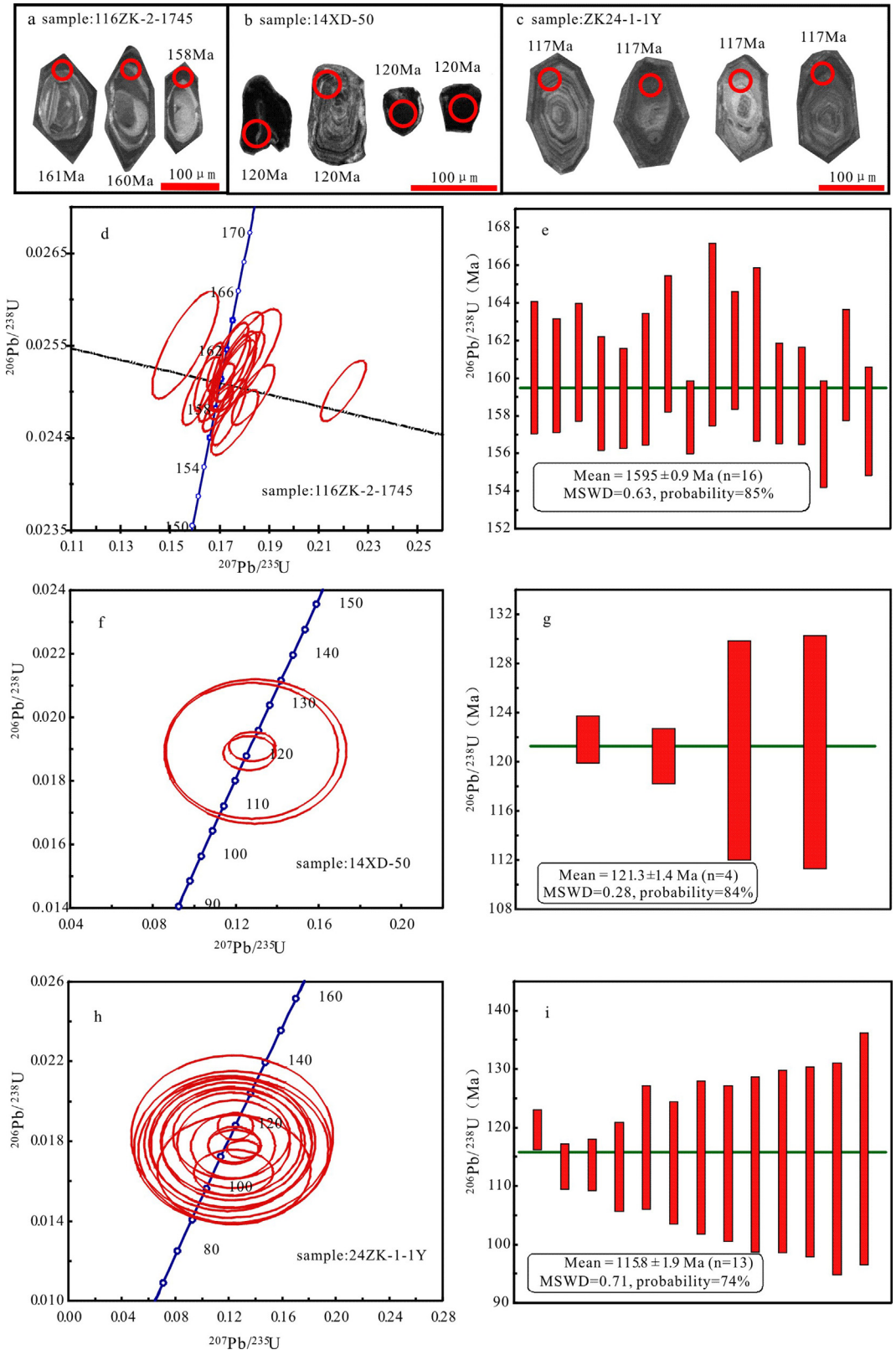

Fig. 7. Representative zircon CL images (a, b, c); the concordia plot for zircon U–Pb dating (d for Linglong granite, f for pre–ore dyke, h for post–ore dyke); the $^{206}Pb/^{238}U$ weighed mean age (e for Linglong granite, g for pre–ore dyke, i for post–ore dyke).

in a drill hole in the nearby Dayingezhuang gold deposit at a depth of −1483 m. At Xiadian, evidence for the presence of the Early Cretaceous hydrothermal activity is represented by the quartz–pyrite–molybdenite veins (Fig. 10). Well defined, high–precision, and accurate isochron ages for five molybdenite samples indicated that molybdenite mineralization occurred at

Table 1
Results of LA–ICPMS zircon U-Pb analysis for Linglong granite, pre-ore and post-ore dykes in the Xiadian gold deposit.

Spot	Pb (ppm)	^{232}Th (ppm)	^{238}U (ppm)	Ratios						Age(Ma)					
				^{207}Pb/^{206}Pb	1σ	^{207}Pb/^{235}U	1σ	^{206}Pb/^{238}U	1σ	^{207}Pb/^{206}Pb	1σ	^{207}Pb/^{235}U	1σ	^{206}Pb/^{238}U	1σ
116zk-2-1745 (Linglong granite)															
1	133	452	929	0.06316	0.00139	1.04075	0.02363	0.11891	0.00097	722.2	48.1	724.3	11.8	724.3	5.6
2	66	562	2348	0.05046	0.00212	0.17595	0.00740	0.02522	0.00035	216.7	93.5	164.6	6.4	160.6	2.2
3	61	444	2237	0.04801	0.00142	0.16568	0.00478	0.02516	0.00030	98.2	70.4	155.7	4.2	160.2	1.9
4	36	124	1339	0.05075	0.00228	0.17800	0.00827	0.02527	0.00031	227.8	105.5	166.3	7.1	160.9	1.9
5	64	703	2301	0.04721	0.00185	0.16269	0.00616	0.02501	0.00030	61.2	88.9	153.1	5.4	159.2	1.9
6	36	18	984	0.04931	0.00268	0.23905	0.01317	0.03513	0.00043	161.2	125.9	217.6	10.8	222.6	2.7
8	53	444	1931	0.05336	0.00204	0.18364	0.00707	0.02496	0.00027	342.7	87.0	171.2	6.1	159.0	1.7
9	47	456	1740	0.05076	0.00223	0.17537	0.00773	0.02513	0.00035	231.6	101.8	164.1	6.7	160.0	2.2
10	34	295	1237	0.05011	0.00245	0.17629	0.00921	0.02543	0.00035	211.2	112.9	164.9	7.9	161.9	2.2
11	106	1787	3675	0.04930	0.00139	0.16943	0.00498	0.02481	0.00019	161.2	66.7	158.9	4.3	158.0	1.2
13	80	950	2801	0.04987	0.00165	0.17446	0.00586	0.02537	0.00031	187.1	77.8	163.3	5.1	161.5	1.9
14	303	194	554	0.16602	0.00302	10.06677	0.18264	0.43874	0.00330	2518.2	31.3	2440.9	16.8	2345.0	14.8
15	138	96	3654	0.05096	0.00118	0.25672	0.00621	0.03642	0.00036	239.0	58.3	232.0	5.0	230.6	2.3
16	36	434	1244	0.05176	0.00347	0.18041	0.01179	0.02534	0.00045	276.0	149.1	168.4	10.1	161.3	2.8
17	6	1	98	0.11727	0.00876	0.91607	0.08144	0.05632	0.00158	1916.7	133.8	660.3	43.2	353.2	9.6
18	71	78	1877	0.04949	0.00152	0.24771	0.00751	0.03618	0.00033	172.3	72.2	224.7	6.1	229.1	2.1
19	98	154	869	0.11727	0.00284	1.54721	0.03748	0.09523	0.00105	1916.7	42.7	949.4	14.9	586.4	6.2
20	83	340	3007	0.06313	0.00203	0.22008	0.00742	0.02501	0.00027	722.2	73.1	202.0	6.2	159.2	1.7
21	83	1134	2934	0.04880	0.00169	0.16879	0.00592	0.02499	0.00026	139.0	81.5	158.4	5.1	159.1	1.6
22	53	206	452	0.06096	0.00220	0.83859	0.03294	0.09933	0.00139	638.9	77.8	618.4	18.2	610.5	8.2
23	48	223	1825	0.05152	0.00225	0.17618	0.00778	0.02467	0.00029	264.9	100.0	164.8	6.7	157.1	1.8
14XD-50 (post-ore dyke)															
1	100	1979	1672	0.04924	0.00283	0.12816	0.00741	0.01908	0.00030	166.8	133.3	122.4	6.7	121.9	1.9
2	98	1910	1787	0.04900	0.00321	0.12677	0.00834	0.01887	0.00036	146.4	148.1	121.2	7.5	120.5	2.3
3	331	247	468	0.17346	0.00995	9.33437	0.60384	0.38094	0.01139	2591.1	96.0	2371.4	59.4	2080.7	53.2
4	719	3434	3472	0.06240	0.00452	0.61576	0.04612	0.07151	0.00197	687.1	155.5	487.2	29.0	445.3	11.8
5	199	2339	3995	0.24642	0.07399	2.43987	0.56313	0.04953	0.00642	3162.0	495.4	1254.4	167.7	311.6	39.4
6	58	257	621	0.05651	0.00618	0.32695	0.03706	0.04204	0.00170	472.3	244.4	287.2	28.4	265.5	10.5
7	94	46	2318	0.05202	0.00631	0.23230	0.02896	0.03248	0.00143	287.1	255.5	212.1	23.9	206.1	8.9
8	309	1007	1302	0.06284	0.00855	0.86898	0.12182	0.10069	0.00508	701.9	292.6	635.0	66.3	618.4	29.7
9	413	249	765	0.11286	0.02062	5.06693	0.95445	0.32491	0.02189	1855.6	336.0	1830.6	161.1	1813.7	106.5
10	45	970	719	0.05017	0.01049	0.12795	0.02750	0.01894	0.00141	211.2	416.6	122.3	24.8	121.0	8.9
11	111	1978	2393	0.04983	0.01083	0.12959	0.02900	0.01893	0.00150	187.1	440.7	123.7	26.1	120.9	9.5
12	278	654	3206	0.06968	0.01626	0.69127	0.18635	0.06218	0.00679	920.4	495.2	533.6	112.3	388.9	41.2
13	52	367	1030	0.07893	0.01963	0.24349	0.06229	0.02284	0.00207	1170.1	504.6	221.3	50.9	145.6	13.1
14	220	526	2614	0.05713	0.01498	0.34755	0.09400	0.04382	0.00423	498.2	492.6	302.9	70.9	276.5	26.1
15	458	1300	2216	0.06701	0.01862	0.93651	0.26879	0.10035	0.01038	838.9	607.4	671.1	141.8	616.5	60.8
ZK24-1-1Y (pre-ore dyke)															
1	66	1134	853	0.05526	0.00369	0.13080	0.00789	0.01760	0.00029	433.4	150.0	124.8	7.1	112.5	1.8
2	26	413	397	0.06539	0.00507	0.15677	0.01262	0.01764	0.00042	787.0	163.0	147.9	11.1	112.7	2.6
3	148	2459	1678	0.04918	0.00341	0.12522	0.00883	0.01875	0.00045	166.8	142.6	119.8	8.0	119.7	2.8
4	50	801	661	0.05310	0.00585	0.12455	0.01304	0.01776	0.00054	331.5	251.8	119.2	11.8	113.5	3.4
5	67	1078	907	0.05186	0.00531	0.12425	0.01285	0.01780	0.00061	279.7	232.4	118.9	11.6	113.8	3.9
6	35	633	515	0.05707	0.00906	0.12367	0.01957	0.01642	0.00076	494.5	355.5	118.4	17.7	105.0	4.8
7	125	993	971	0.16260	0.02447	0.46926	0.07381	0.02054	0.00112	2483.0	255.4	390.7	51.1	131.1	7.1
8	76	1275	945	0.05140	0.00836	0.12345	0.02073	0.01775	0.00106	257.5	337.0	118.2	18.7	113.4	6.7
9	71	78	75	0.10671	0.01841	3.93103	0.70654	0.27029	0.01766	1744.1	320.4	1620.1	146.5	1542.3	89.6
10	835	13075	4501	0.12819	0.02420	0.35727	0.07110	0.01965	0.00138	2073.1	337.5	310.2	53.2	125.5	8.7
11	17	202	361	0.05215	0.01219	0.12214	0.02884	0.01828	0.00142	300.1	453.7	117.0	26.1	116.8	9.0
12	117	1961	1410	0.05081	0.01104	0.12389	0.02799	0.01786	0.00145	231.6	501.8	118.6	25.3	114.1	9.2
13	246	308	881	0.10939	0.02491	2.81468	0.67334	0.18355	0.01668	1790.7	425.9	1359.5	181.1	1086.4	90.8
14	457	158	461	0.19719	0.04774	11.74978	2.96300	0.43210	0.03965	2802.8	406.9	2584.7	240.4	2315.2	178.5
15	37	577	539	0.05160	0.01435	0.12204	0.03476	0.01800	0.00179	333.4	472.2	116.9	31.5	115.0	11.4
16	91	1387	1089	0.05109	0.01406	0.12362	0.03536	0.01784	0.00184	255.6	533.3	118.3	32.0	114.0	11.7
17	48	672	1025	0.05566	0.01633	0.12432	0.03783	0.01657	0.00181	438.9	548.1	119.0	34.2	106.0	11.5
18	30	407	462	0.05152	0.01622	0.12220	0.03973	0.01781	0.00207	264.9	596.2	117.1	36.0	113.8	13.1
19	60	994	792	0.04987	0.01597	0.12275	0.04093	0.01790	0.00215	187.1	1012.9	117.6	37.0	114.4	13.6
20	35	327	1085	0.04916	0.01636	0.11974	0.04145	0.01789	0.00224	153.8	637.0	114.8	37.6	114.3	14.2
21	17	299	273	0.07208	0.02613	0.16759	0.06165	0.01844	0.00245	988.0	602.8	157.3	53.7	117.8	15.5
22	51	745	771	0.05194	0.01899	0.12357	0.04700	0.01755	0.00240	283.4	671.8	118.3	42.5	112.1	15.2
23	107	1827	1066	0.05021	0.01903	0.12299	0.04859	0.01769	0.00252	205.6	699.9	117.8	44.0	113.1	15.9
24	79	905	1967	0.04919	0.01918	0.12269	0.04980	0.01823	0.00268	166.8	712.9	117.5	45.1	116.5	17.0

124.8 ± 2.1 Ma (2σ, MSWD = 0.10). These molybdenite–bearing veins were discovered in pegmatite, and as such they may be magmatic in origin. As an incompatible element in a crystallizing magma (Candela and Holland, 1984; Keppler and Wyllie, 1991), molybdenum is often accumulated in the residual melts (Audétat, 2010). As a result, Mo–rich fluids can be expected to exsolve from magmas (Seo et al., 2012). The molybdenite mineralization at Xiadian closely followed the intrusion of the Guojialing granodiorite (~130 Ma). Since there are no other hydrothermal events during this time at Jiaodong, it is postulated

Table 2
Re–Os data of molybdenite in the Xiadian gold deposit.

Sample No.	Sample weight(g)	Re (ng/g)		Common Os (ng/g)		^{187}Re (ng/g)		^{187}Os (ng/g)		Model age (Ma)	
		Measured	Error	Measured	Error	Measured	Error	Measured	Error	Measured	Error
14XD-35-1	0.01963	7834	51.9	0.050	0.009	4924	32.635	10.377	0.060	126.4	1.7
14XD-35-2	0.01940	11094	72.3	0.050	0.0085	6973	45.419	14.652	0.086	126.0	1.7
14XD-35-3	0.01937	9564	72.90	0.052	0.0115	6011	45.820	12.619	0.082	125.9	1.8
14XD-35-4	0.01960	107130	1980.08	0.044	0.010	67333	1244.599	140.417	0.821	125.0	2.7
14XD-35	0.02113	12101	83	0.034	0.0127	7606	52.363	15.924	0.108	125.5	1.7

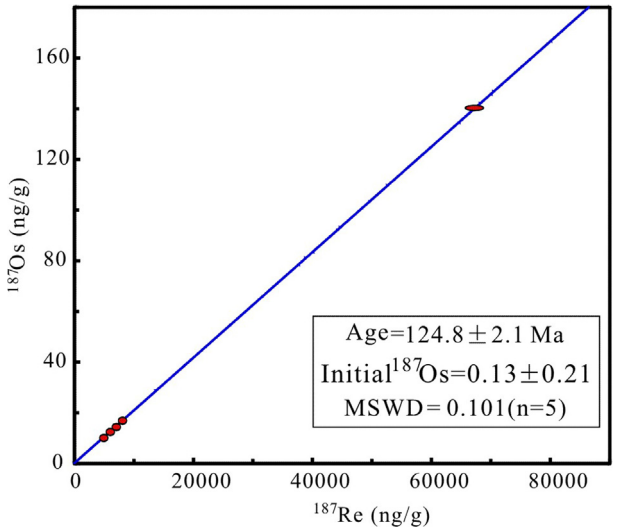

Fig. 8. Molybdenite Re–Os isochron diagram for five molybdenite samples of the Xiadian gold deposit. Decay constant: $\lambda(^{187}Re) = 1.666 \times 10^{-11}$ year^{-1} (Smoliar et al., 1996), uncertainties are absolute at 2σ.

that the molybdenite originated from differentiation of the Guojialing granodiorite. Moreover, molybdenite mineralization often has a close relationship with emplacement of igneous rocks that host the mineralization, as well as with hydrothermal processes that occurred during this emplacement (Xiao et al., 2014). Given the presence of the Guojialing granodiorite at Dayingezhuang gold deposit (15 km north of Xiadian), we infer that Guojialing granodiorite might be concealed at depth in the Xiadian gold deposit, serving as the source of the molybdenite mineralization. In addition, many studies support that crustal and mantle reservoirs within the subduction zone environments have distinct Re contents so that deposits with a mantle component should have higher Re contents compared to those with a crustal origin (Mao et al., 2008; Voudouris et al., 2009). Stein et al. (2001) proposed that deposits involving mantle underplating or melting of mafic and ultramafic rocks, usually contain high Re concentrations. In contrast, ore deposits originating from crustal sources or sedimentary sequences poor in organic matter may have lower Re concentrations. Generally, the Re content of a mantle source is 100 to 1000 ppm; the Re content of the mixture source of mantle and crust is 10 to 100 ppm; while for the crust source, the average Re content is several ppm (Mao et al., 2003). The Re contents of molybdenite from the Xiadian gold deposit range from 7.83 to 107.13 ppm (averaging 29.54 ppm) suggesting a mixing source between the mantle and crust, suggesting that the Guojialing granodiorite formed by the remelting of Archean lower crust with addition of mantle components (Yang et al., 2012).

Table 3
Results of in-situ LA–ICPMS U-Pb analysis for hydrothermal monazite in the Xiadian gold deposit.

Analysis No.	Isotopic ratios								^{207}Pb-corr. Age(Ma)	
	^{207}Pb/^{206}Pb	1σ	^{207}Pb/^{235}U	1σ	^{206}Pb/^{238}U	1σ	^{208}Pb/^{232}Th	1σ	^{206}Pb/^{238}U	1σ
1	0.21100	0.01234	0.70710	0.03314	0.02430	0.00091	0.00611	0.00007	125	6
2	0.12496	0.01151	0.34568	0.02823	0.02006	0.00090	0.00603	0.00007	116	6
3	0.46848	0.01648	2.42212	0.05374	0.03750	0.00114	0.00700	0.00009	119	7
4	0.50084	0.01992	2.77251	0.06875	0.04015	0.00138	0.00694	0.00010	117	9
5	0.56806	0.01847	3.99888	0.07930	0.05105	0.00151	0.00847	0.00013	123	9
6	0.46049	0.01546	2.37964	0.05089	0.03748	0.00109	0.00752	0.00011	121	7
7	0.35835	0.01585	1.45940	0.04389	0.02954	0.00104	0.00634	0.00008	119	7
8	0.49689	0.01890	2.83620	0.06769	0.04140	0.00137	0.00744	0.00011	122	8
9	0.50659	0.01798	2.86208	0.06375	0.04098	0.00127	0.00685	0.00009	118	8
10	0.37301	0.01275	1.56476	0.03581	0.03043	0.00086	0.00679	0.00009	119	5
11	0.51269	0.01846	3.03724	0.06807	0.04297	0.00136	0.00785	0.00012	122	8
12	0.43195	0.01686	2.08351	0.05221	0.03498	0.00116	0.00662	0.00009	121	7
13	0.13144	0.01142	0.39209	0.02998	0.02164	0.00094	0.00624	0.00009	124	6
14	0.22155	0.01275	0.73990	0.03367	0.02422	0.00092	0.00663	0.00011	123	6
15	0.44426	0.02273	2.17961	0.07262	0.03558	0.00150	0.00685	0.00011	119	9
16	0.34519	0.01749	1.43723	0.04975	0.03020	0.00120	0.00719	0.00013	124	8
17	0.11401	0.01171	0.31460	0.02934	0.02001	0.00091	0.00636	0.00012	118	6
18	0.31355	0.02071	1.22693	0.05837	0.02838	0.00138	0.00660	0.00012	124	9
19	0.29771	0.02455	1.10810	0.06738	0.02700	0.00158	0.00654	0.00011	121	10
20	0.07826	0.01225	0.20713	0.03061	0.01920	0.00103	0.00632	0.00016	118	7
21	0.08880	0.00987	0.23484	0.02349	0.01918	0.00098	0.00582	0.00012	117	6
22	0.36806	0.01981	1.52584	0.05594	0.03007	0.00127	0.00762	0.00015	118	8
23	0.33060	0.01912	1.26197	0.05145	0.02769	0.00121	0.00647	0.00011	117	8
24	0.26017	0.01845	0.88382	0.04721	0.02464	0.00121	0.00648	0.00010	117	8
25	0.58069	0.01989	4.14499	0.08535	0.05178	0.00161	0.01049	0.00019	120	10
26	0.22798	0.02150	0.73950	0.05345	0.02353	0.00149	0.00627	0.00012	118	9
27	0.54140	0.01917	3.42982	0.07532	0.04595	0.00144	0.00945	0.00016	120	9

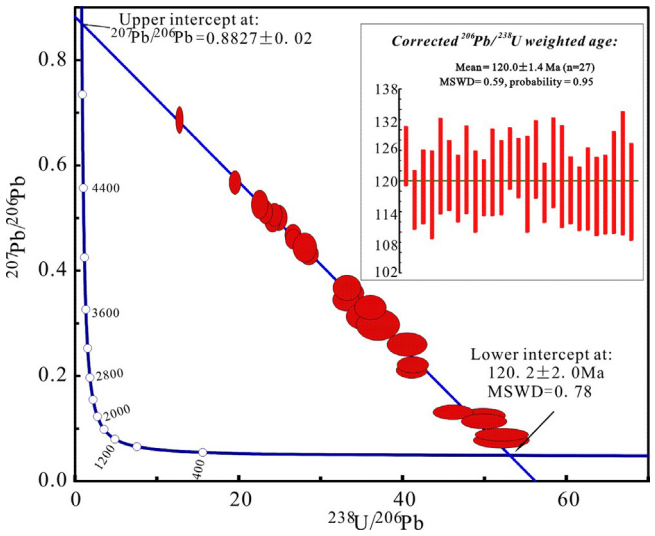

Fig. 9. Monazite U–Pb Tera–Wasserburg Concordia diagrams (a) and weighed mean age (b) of the Xiadian gold deposit.

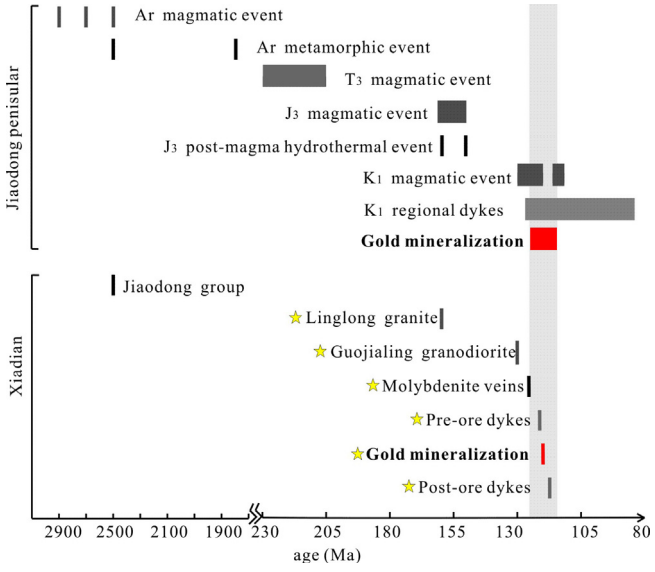

Fig. 10. Geological event in the Jiaodong Peninsula and Xiadian gold deposit The star marked age data are from this study, the other are from previous study. The Ar magmatic event datas are from Wu et al. (2013, 2014) and Yang and Li (2008). Ar metamorphic event datas are from Jahn et al. (2008) and Liu et al. (2013), T3 magmatic event datas are from Chen et al. (2003) and Yang et al. (2007), J3 magmatic event datas are from e.g. Wang et al. (1998) and Yang et al. (2012), J3 post-magma hydrothermal event data are from Ding et al. (2012), Liu et al. (2011) and Wen et al. (2015b), K1 magmatic event and Guojialing granodiorite data are from Yang et al. (2012), K1 regional dykes are from Cai et al. (2013) and Yang and Zhou (2001), Gold mineralization in Jiaodong peninsular are from Hu et al. (2004) and Li et al. (2003, 2006, 2008), Jiaodong group data are from e.g. Wu et al. (2013).

The zircon U-Pb dating indicates that the ages of the dykes in the Jiaodong Peninsula range from 127 to 87 Ma (Cai et al., 2013; Liu et al., 2004; Wang et al., 1998; Yang et al., 2013). Our work in the Xiadian gold deposit shows that the U–Pb ages of the pre-ore diorite dykes and post-ore quartz diorite dykes are 121.3 ± 1.4 Ma (2σ, MSWD = 0.28) and 115.8 ± 1.9 Ma (2σ, MSWD = 0.71), respectively. These ages overlap the intrusion of the regional Early Cretaceous dykes (Fig. 10). Liu et al. (2004) showed that the emplacement of the dykes correlated to the Cretaceous crustal extension in the Jiaodong Peninsula.

6.2. Timing of gold mineralization

A recent sericite and muscovite $^{40}Ar/^{39}Ar$ study on the nearby Dayingezhuang gold deposit and zircon fission track dating on the Xiadian gold deposit yielded ages of ~130 Ma, which was considered to be the mineralization ages of the respective gold deposits (Yang et al., 2014, 2016). Yang et al. (2016) further proposed that these mineralization events occurred 10 million years earlier (ca. 120 Ma) than other Jiaodong gold deposits, and therefore represent the earliest gold mineralization in Jiaodong.

However, their Ar-Ar results might be unreliable due to several inherent problems. Firstly, excess argon is common in granite intrusion–related hydrothermal systems (Kelley et al., 1986; Turner et al., 1993). Secondly, later fluids reworking the altered rocks and minerals can interfere with the parent/daughter isotopic system, leading to the excess or loss of Ar in the sericite (Qiu et al., 2008; Tartese et al., 2011). Thirdly, loss of ^{39}Ar by recoil during irradiation in the experiment is inevitable (Li et al., 2003). The presence of inherited argon and a combination of excess and inherited argon would yield an older age (Hopp et al., 2008; Kelley and Wartho, 2000). Similarly for the ZFT dating, several problems can lead to unreliable ages. Closure temperatures for fission tracks in zircon are below those of conventional geochronometers, so they are more useful in the analysis of low temperature events (generally 240 ± 50 °C for zircon) (Gallagher et al., 1998), but previous fluid inclusion studies in the Xiadian gold deposit showed that the temperature of gold mineralization ranges from 140 °C to 380 °C with most concentrated in 240 °C to 300 °C (Xu et al., 2013). Thus, the ZFT cannot effectively record the age of gold mineralization. In addition, each track is actually represented by a different age and has experienced a different fraction of the thermal history of the sample (Gallagher et al., 1998). The broad range of ZFT central ages of ore samples (130.8 ± 3.6 Ma (1σ) to 114.9 ± 8.7 Ma (1σ)) in the Xiadian gold deposit (Yang et al., 2016) reflects a complex thermal history. Therefor it is premature to exclude the highly precise ZFT age of 114.9 ± 8.7 Ma (though the number of zircons is small) and choose the 130 Ma to represent the age of gold mineralization in the study from Yang et al. (2016).

Previous geochronological studies of gold mineralization in the Jiaodong district employed the indirect dating method on alteration minerals and quartz, for example, Rb–Sr, K-Ar and $^{40}Ar/^{39}Ar$ dating on sericite/muscovite (Li et al., 2003, 2006; Sun et al., 1995; Zhang et al., 1994) and $^{40}Ar/^{39}Ar$ on quartz (Zhang et al., 2002) or direct dating method on sulfide minerals (Rb-Sr dating) (Li et al., 2008; Yang and Zhou, 2001) and hydrothermal zircon (U-Pb dating) (Hu et al., 2004). These studies indicated that gold mineralization in the Jiaodong district occurred between 125 and 114 Ma. However, no direct and in-situ dating results have been reported yet. As monazite has a robust isotopic system (U-Th-Pb) with high closure temperatures (700–750 °C, Smith and Giletti, 1997; Suzuki and Adachi, 1994), it is an ideal mineral for dating hydrothermal deposits (Janots et al., 2014). Eliminating mixing of distinct systems is also available from the in-situ U–Pb dating of monazite. The monazite closely associated with pyrite, quartz and sericite in quartz–polymetallic sulfide veins indicates that it was formed during the Stage III hydrothermal mineralization event. Monazite U-Pb dating in this study provides the first direct in-situ age (120.0 ± 1.4 Ma) for the timing of gold mineralization in the Jiaodong gold deposit. U–Pb ages of the pre–ore and post–ore dykes are 121.3 ± 1.4 Ma (2σ, MSWD = 0.28) and 115.8 ± 1.9 Ma (2σ, MSWD = 0.71), respectively. These data constrain the mineralization age between 121 Ma and 115 Ma and show good concordance with the monazite U-Pb dating result, verifying the effectiveness of the in-situ monazite U-Pb dating. The age of gold mineralization in the Xiadian gold deposit, combined with

published data from other gold deposits, vigorously constrain the gold mineralization in the Jiaodong district at ca. 120 Ma (Fig. 10).

6.3. Implications for the origin of gold mineralization

The presence of metamorphosed Jiaodong Group exposed in the Xiadian gold deposit suggests that this region experienced a ~2.5 Ga metamorphic event. Considering that metamorphic ages of the metamorphic rocks in the study region are about 2 billion years older than the mineralization ages of the gold deposits, the gold mineralization cannot be related with the metamorphism. In addition, the relatively high-grade metamorphic conditions (amphibolite to granulite facies) in the study region suggest that, unlike most greenschist-facies terranes that host orogenic gold deposits, the metamorphic rocks in the Jiaodong gold deposit had insufficient volatiles to transport gold (Goldfarb and Santosh, 2014)

Gold mineralization at Xiadian postdates the intrusion of Linglong granitoids and Guojialing granodiorite (~130 Ma, Yang et al., 2012). In addition, the temperature of the ore-forming fluid system for gold deposits (mostly 200–350 °C, Fan et al., 2003; Wen et al., 2015a) is substantially lower than that of magmas (>573 °C) and the density of the ore-forming fluids is substantially lower than that of the magma (Song et al., 2015). Thus, we exclude the possibility that ore fluids were derived from these intrusions. Petrographic analyses and SEM imaging show that the molybdenite formed together with quartz and pyrite. However, it should be noted that the gold-bearing veins contain no molybdenite. In addition, the presence of the pre-ore dykes (121.3 ± 1.4 Ma (2σ, MSWD = 0.28)) indicates that the timing of the gold mineralization cannot be earlier than 121 Ma. Considering the above observations, it is likely that the molybdenite mineralization represents a distinct hydrothermal fluid event to the one that precipitated gold.

Though the hydrothermal fluids responsible for the precipitation of molybdenite were not the ore-forming fluids, these hydrothermal fluids may get involved in the forming of the ore-forming fluids. Guojialing granodiorite is the host rock to several large gold deposits, such as Xincheng, Jiehe, Shangzhuang and Sanshandao, and the age (130 ~126 Ma, Wang et al., 1998) is close to that the gold mineralization (especially in previous geochronological studies, for example, some are dated at ~128 Ma, Zhang et al. (2003)). Li et al. (2007) proposed that the formation of the gold deposits is closely related to Mesozoic magmatic activity and that the post–magmatic hydrothermal activity of the Guojialing granodiorite is the direct cause for gold precipitation. In addition, petrological and geochemical features suggest that Guojialing granodiorite was responsible for gold to be transferred into melt and fluid phases (Xu et al., 1992; Chen et al., 1993). The ideal petrological and geochemical features of granitoid plutons that are favorable for gold mineralization are mainly in their low differentiation index, indicated by Differentiation Index (DI) <88, high Ba/Sr and K/Rb values, ranging from 1.87 to 4.45 and from 423 to 1063, respectively; and low Rb/Sr values ranging from 0.05 to 0.13 (Xu et al., 1992). Chen et al. (1993) found that the Cretaceous Guojialing granodiorite coincide with those features except for the contents of iron group elements Fe, Cr, Ni, and V which were slightly lower, and F and Cl were slightly higher which would be favorable for gold mineralisation. Furthermore, the oxidizing condition, plus high contents of volatile and alkaline compositions are profitable for gold reacting and getting transferred into melt and fluid phases (Chen et al., 1993). Interestingly, Guojialing granodiorite exhibits similar features concerning high volatile contents and alkaline signatures which have been deduced from the presence of the large K-feldspar phenocrysts, alkaline mineral and oxides, and the high formation temperature of 850 °C to 500 °C (Chen et al., 1993). Thus, the forming condition of Guojialing granodiorite may also favor Au reacting and getting transferred into melt and fluid phases (Chen et al., 1993; Li et al., 2014). Herein, the molybdenite was associated with the gold-bearing fluids as it differentiated from Guojialing granodiorite. Regarding the duration of hydrothermal activity, Burnard and Polya (2004) suggested that several pulses of (mantle-derived) heat may keep the hydrothermal cell active and prolong the duration of the hydrothermal system. For example, hydrothermal activity at Panasqueira is thought to have been active for 4 million years (between 296 and 292 Ma, Snee et al., 1988), considerably longer than the length of time that a single intrusion could sustain. Due to the widespread dykes in the Xiadian gold deposit, we assume that the pulses of mantle-derived heat would sustain molybdenite mineralization activity for several million years and extend to the time of the gold mineralization.

During the period of gold mineralization (~120 Ma), the eastern NCC witnessed craton destruction or decratonization (Wu et al., 2005; Yang and Li, 2008; Zhu et al., 2012, 2015), regional tectonic inversion and significant lithosphere thinning, strong crust–mantle interaction and asthenospheric upwelling (Cai et al., 2013; Menzies et al., 1993). Simultaneously, lithospheric thinning led to partial melting and dehydration of the lithospheric mantle and lower crust as the temperature increased (Yang et al., 2003). Therefore, the hydrothermal fluid carrying the molybdenite would inevitably be contaminated by mantle or crustal material if it was sustained for about 4–5 million years. Previous studies also show that the fluids and the gold are from multiple sources (Fan et al., 2007; Goldfarb and Santosh, 2014). Molybdenum-bearing hydrothermal fluids mixing with mantle or crustal source materials may generate the ore-forming fluids for the Xiadian gold deposit.

The hydrogen, oxygen, carbon and sulfur stable isotope analyses demonstrate that the initial ore-forming fluids were composed mainly of magmatic water, and mixed with meteoric water during later metallogenic processes (e.g., Fan et al., 2003). Thus, Fan et al. (2003) and Zhou et al. (2003) considered that the fluids responsible for mineralization in the Jiaodong gold province were derived from fluids degassed from mafic to intermediate magmas because the intrusion of these dykes and the gold mineralization share similar ages. Considering the widespread distribution of mafic dykes and close temporal relationship with the gold mineralization, they might play a role in providing the source of the ore fluids from mantle–derived magmas for the gold mineralization in the Xiadian gold deposit (Fan et al., 2003; Wen et al., 2015a).

7. Conclusions

Based on the study of the geology, timing of granite emplacement, dykes, molybdenite and gold mineralization, we have reached the following main conclusions:

(1) Linglong granite has a crystallization age of ~160 Ma as defined by zircon U-Pb dating. Re–Os dating shows that molybdenite mineralization in pegmatite occurred at 124.8 ± 2.1 Ma. The Re contents of the Xiadian molybdenite range from 7.83 to 107.13 ppm (averaging 29.54 ppm) suggesting a mixed source between the mantle and crust, suggesting that the Guojialing granodiorite was formed by the remelting of Archean lower crust with addition of mantle components. The molybdenite may be derived from the Guojialing granodiorite because (1) the molybdenite-quartz vein have close temporal and spatial relationship with Guojialing granodiorite (observed in the nearby Dayingezhuang gold deposit located 15 km away and dated at ~130 Ma) and (2) the molybdenite-quartz vein display similar mixing sources with Guojialing granodiorite.

(2) Zircon U-Pb dating of pre-ore dykes and post-ore dykes at the Xiadian gold deposit yield ages of 121.3 ± 1.4 Ma and 115.8 ± 1.9 Ma, respectively, constraining the age of gold mineralization to 121–115 Ma. The U-Pb dating of the monazite from quartz–polymetallic sulfides veins suggests the gold mineralization in the Xiadian deposit is 120.0 ± 1.4 Ma.
(3) Achaean metamorphosed Jiaodong Group, the Linglong granite and the Guojialing granodiorite are excluded as the direct sources for the ore-forming fluid due to the wide age gap between these intrusions and the gold mineralization. The molybdenum-bearing hydrothermal fluids which most likely originated from the Guojialing granodiorite predate gold mineralization.

Acknowledgements

We gratefully acknowledge Dr. Paul Duuring and Dr. Alistair White for their constructive reviews and valuable comments which greatly contributed to the improvement of the manuscript. Special thanks are due to the managements and staffs of the Shandong Zhaojin Group and the Xiadian Mine for their hospitality during fieldworks. We would also like to thank Drs. Xin Yan and Sai-Hong Yang for their helps with the BSE and CL imaging, Dr. Li-Min Zhou for helps with molybdenite Re–Os dating analysis and Dr. Xiao-Chun Li for considerable efforts in processing and interpreting of monazite LA–ICPMS U-Pb dating. This study was financially supported by the National Natural Science Foundation of China (41672094) and National Key Research and Development Program (No. 2016YFC0600105).

References

Alagna, K.E., Petrelli, M., Perugini, D., Poli, G., 2008. Micro-analytical Zircon and monazite U-Pb isotope dating by laser ablation-inductively coupled plasma-quadrupole mass spectrometry. Geostand. Geoanal. Res. 32, 103–120.
Aleinikoff, J.N., Schenck, W.S., Plank, M.O., Srogi, L., Fanning, C.M., Kamo, S.L., Bosbyshell, H., 2006. Deciphering igneous and metamorphic events in high-grade rocks of the Wilmington Complex, Delaware: Morphology, cathodoluminescence and backscattered electron zoning, and SHRIMP U-Pb geochronology of zircon and monazite. Geol. Soc. Am. Bull. 118, 39–64.
Audétat, A., 2010. Source and evolution of molybdenum in the porphyry Mo (–Nb) deposit at Cave Peak. Texas. J. Petrol. 10, 037.
Burnard, P.G., Polya, D.A., 2004. Importance of mantle derived fluids during granite associated hydrothermal circulation: He and Ar isotopes of ore minerals from Panasqueira. Geochim. Cosmochim. Acta 68, 1607–1615.
Cai, Y.C., Fan, H.R., Santosh, M., Liu, X., Hu, F.F., Yang, K.F., Lan, T.G., Yang, Y.H., Liu, Y. S., 2013. Evolution of the lithospheric mantle beneath the southeastern North China Craton: constraints from mafic dikes in the Jiaobei terrain. Gondwana Res. 24, 601–621.
Candela, P.A., Holland, H.D., 1984. The partitioning of copper and molybdenum between silicate melts and aqueous fluids: Geochim. Cosmochim. Acta 48, 373–380.
Charles, N., Augier, R., Gumiaux, C., Monié, P., Chen, Y., Faure, M., Zhu, R.X., 2013. Timing, duration and role of magmatism in wide rift systems: insights from the Jiaodong Peninsula (China, East Asia). Gondwana Res. 24, 412–428.
Chen, G.Y., Sun, D.S., Zhou, X.R., Shao, W., Gong, R.T., Shao, Y., 1993. Genetic Mineralogy and Gold Mineralization of Guojialing Granodiorite in Jiaodong Region. China University of Geosciences Press, pp. 1–230 (in Chinese with English abstract).
Chen, J.F., Xie, Z., Li, H.M., Zhang, X.D., Zhou, T.X., Park, Y.S., Ahn, K.S., Chen, D.G., Zhang, X., 2003. U-Pb zircon ages for a collision-related K-rich complex at Shidao in the Sulu ultrahigh pressure terrane. China. Geochem J. 37, 35–46.
Deng, J., Wang, Q.F., Wan, L., Yang, L.Q., Gong, Q.J., Zhao, J., Liu, H., 2009. Self–similar fractal analysis of gold mineralization of Dayingezhuang disseminated–veinlet deposit in Jiaodong gold province. China. J. Geochem. Explor. 102, 95–102.
Deng, J., Chen, Y.M., Liu, Q., Yang, L.Q., 2010. The Gold Metallogenic System and Mineral Resources Exploration of Sanshandao Fault Zone. Geological Press, Shandong Province, Beijing, pp. 1–371 (in Chinese).
Ding, Z.J., Sun, F.Y., Liu, J.H., Liu, D.H., Li, B.L., Zhang, P.J., Qian, Y., Li, J., 2012. Re–Os dating of molybdenites from the Xingjiashan molybdenum–tungsten deposit in Jiaodong Peninsula, China and its geological significance. Acta Petrol. Sin. 28, 2721–2732.
Du, A.D., Wu, S.Q., Sun, D.Z., Wang, S., Qu, W.J., Markey, R., Stain, H., Morgan, J., Malinovskiy, D., 2004. Preparation and certification of Re–Os dating reference materials: molybdenites HLP and JDC. Geostand. Geoanal. Res. 28, 41–52.
Fan, H.R., Zhai, M.G., Xie, Y.H., Yang, J.H., 2003. Ore–forming fluids associated with granite hosted gold mineralization at the Sanshandao deposit, Jiaodong gold province. China. Miner Depos. 38, 739–750.
Fan, H.R., Hu, F.F., Yang, J.H., Zhai, M.G., 2007. Fluid evolution and large-scale gold metallogeny during Mesozoic tectonic transition in the Jiaodong Peninsula, eastern China. Geochem. Soc. Lond. Spec. Publ. 280, 303–316.
Gallagher, K., Brown, R., Johnson, C., 1998. Fission track analysis and its applications to geological problems. Annu. Rev. Earth. Pl. Sc. 26, 519–572.
Gao, S., Rudnick, R.L., Yuan, H.L., Liu, X.M., Liu, Y.S., Xu, W.L., Wang, Q.H., 2004. Recycling lower continental crust in the North China craton. Nature 432, 892–897.
Goldfarb, R.J., Santosh, M., 2014. The dilemma of the Jiaodong gold deposits: are they unique? Geosci Fron. 5, 139–153.
Goldfarb, R.J., Groves, D.I., Gardoll, D., 2001. Orogenic gold and geologic time: a global synthesis. Ore Geol Rev. 18, 1–75.
Goldfarb, R.J., Hart, C.J.R., Davis, G., Groves, D.I., 2007. East Asian gold–deciphering the anomaly of Phanerozoic gold in Precambrian cratons. Econ. Geol. 102, 341–346.
Hopp, J., Trieloff, M., Brey, G.P., Woodland, A.B., Simon, N.S.C., Wijbrans, J.R., Siebel, W., Reitter, E., 2008. $^{40}Ar/^{39}Ar$–ages of phlogopite in mantle xenoliths from South African kimberlites: evidence for metasomatic mantle impregnation during the Kibaran orogenic cycle. Lithos 106, 351–364.
Hu, F.F., Fan, H.R., Yang, J.H., Wan, Y.S., Liu, D.Y., Zhai, M.G., Jin, C.W., 2004. Hydrothermal U-Pb zircon Shrimp dating ore–forming age of the lode gold–quartz–sulphide veins in Rushan, Jiaodong Peninsula. Chinese Sci Bull. 49, 1191–1198.
Huang, J., Zheng, Y.F., Zhao, Z.F., Wu, Y.B., Zhou, J.B., Liu, X., 2006. Melting of subducted continent: element and isotopic evidence for a genetic relationship between Neoproterozoic and Mesozoic granitoids in the Sulu orogen. Chem Geol. 229, 227–256.
Jahn, B.M., Liu, D.Y., Wan, Y.S., Song, B., Wu, J.S., 2008. Archean crustal evolution of the Jiaodong Peninsula, China, as revealed by zircon SHRIMP geochronology, elemental and Nd-isotope geochemistry. Am J Sci. 308, 232–269.
Janots, E., Gnos, E., Berger, A., Whitehouse, M., 2014. High spatial resolution dating of hydrothermal monazite from Alpine clefts. EGU Gen. Assembly Conf. Abstr. 16, 7145.
Jiang, Y.H., Jiang, S.Y., Ling, H.F., Ni, P., 2010. Petrogenesis and tectonic implications of Late Jurassic shoshonitic lamprophyre dikes from the Liaodong Peninsula. NE China. Miner Petrol. 100, 127–151.
Jiang, P., Yang, K.F., Fan, H.R., Liu, X., Cai, Y.C., Yang, Y.H., 2016. Titanite-scale insights into multi-stage magma mixing in Early Cretaceous of NW Jiaodong terrane, North China Craton. Lithos 258, 197–214.
Kazimoto, E.O., Schenk, V., Appel, P., 2015. The age of Au–Cu–Pb-bearing veins in the poly-orogenic Ubendian Belt (Tanzania): U-Th–total Pb dating of hydrothermally altered monazite. Contrib Mineral Petr. 169, 1–18.
Kelley, S.P., Wartho, J.A., 2000. Rapid kimberlite ascent and the significance of Ar–Ar ages in xenolith phlogopites. Science 289, 609–611.
Kelley, S.P., Turner, G., Butterfield, A.W., Shepherd, T.J., 1986. The source and significance of argon in fluid inclusions from areas of mineralization. Earth Planet. Sci. Lett. 79, 303–318.
Keppler, H., Wyllie, P.J., 1991. Partitioning of Cu, Sn, Mo, W, U, and Th between melt and aqueous fluid in systems halpogranite–H_2O–HCl and halogranite–H_2O–HF. Contrib Mineral Petr. 109, 139–150.
Košler, J., Simonetti, A., Sylvester, P.J., Cox, R.A., Tubrett, M.N., Wilton, D.H.C., 2003. Laser-ablation ICP–MS measurements of Re/Os in molybdenite and implications for Re–Os geochronology. Can Mineral. 41, 307–320.
Li, J.W., Vasconcelos, P.M., Zhang, J., Zhou, M.F., Zhang, X.J., Yang, F.H., 2003. $^{40}Ar/^{39}Ar$ constraints on a temporal link between gold mineralization, magmatism, and continental margin transtension in the Jiaodong gold province, eastern China. J. Geol. 111, 741–751.
Li, J.W., Vasconcelos, P.M., Zhou, M.F., Zhao, X.F., Ma, C.Q., 2006. Geochronology of the Pengjiakuang and Rushan gold deposits, eastern Jiaodong gold province, northeastern China: implications for regional mineralization and geodynamic setting. Econ Geol. 101, 1023–1038.
Li, S.X., Liu, C.C., An, Y.H., Wang, W.C., Huang, T.L., Yang, C.H., 2007. Geology of Gold Deposits in Shandong Peninsula. Geological Publishing House, Beijing., 102–111 (in Chinese)
Li, Q.L., Chen, F.K., Yang, J.H., Fan, H.R., 2008. Single grain pyrite Rb–Sr dating of the Linglong gold deposit, eastern China. Ore Geol Rev. 34, 263–270.
Li, L., Santosh, M., Li, S.R., 2014. The 'Jiaodong type'gold deposits: characteristics, origin and prospecting. Ore Geol Rev 65, 589–611.
Liu, S., Hu, R.Z., Zhao, J.H., Feng, C.X., 2004. K-Ar geochronology of Mesozoic mafic dikes in Shandong Province, Eastern China: implications for crustal extension. Acta Geol. Sin. 78, 1207–1213.
Liu, S., Hu, R.Z., Gao, S., Feng, C.X., Yu, B.B., Qi, Y.Q., Wang, T., Feng, G.Y., Coulson, I.M., 2009. Zircon U-Pb age, geochemistry and Sr–Nd–Pb isotopic compositions of adakitic volcanic rocks from Jiaodong, Shandong Province, Eastern China: constraints on petrogenesis and implications. J. Asian Earth Sci. 35, 445–458.
Liu, Y.S., Gao, S., Hu, Z.C., Gao, C.G., Zong, K., Wang, D., 2010. Continental and oceanic crust recycling–induced melt–peridotite interactions in the Trans-North China Orogen: U-Pb dating, Hf isotopes and trace elements in zircons of mantle xenoliths. J. Petrol. 51, 537–571.
Liu, J., Song, M.C., Wang, M.Y., Li, S.Y., Zhou, M.L., Ni, S.J., Zhang, C.J., Ding, Z.J., Yue, Y. P., 2011. Re–Os dating of molybdenites from Shangjiazhuang molybdenum gold deposit in Jiaodong Peninsula, China and its geological significance. Miner Depos. 40, 483–485.

Liu, Z.C., Wu, F.Y., Yang, Y.H., Yang, J.H., Wilde, S.A., 2012. Neodymium isotopic compositions of the standard monazites used in U-Th-Pb geochronology. Chem. Geol. 334, 221–239.
Liu, J., Liu, F., Ding, Z., Liu, C., Yang, H., Liu, P., Wang, F., Meng, E., 2013. The growth, reworking and metamorphism of early Precambrian crust in the Jiaobei terrane, the North China Craton: constraints from U-Th–Pb and Lu–Hf isotopic systematics, and REE concentrations of zircon from Archean granitoid gneisses. Precambr Res. 224, 287–303.
Ludwig, K.R., 2012. Isoplot/Ex, v. 3.75, vol. 5. Geochronology Center Special Publication, Berkeley.
Ma, L., Jiang, S.Y., Dai, B.Z., Jiang, Y.H., Hou, M.L., Pu, W., Xu, B., 2013. Multiple sources for the origin of Late Jurassic Linglong adakitic granite in the Shandong Peninsula, eastern China: zircon U-Pb geochronological, geochemical and Sr–Nd–Hf isotopic evidence. Lithos 162, 175–194.
Mao, J.W., Du, A.D., Seltmann, R., Yu, J.J., 2003. Re-Os ages for the Shameika porphyry Mo deposit and the Lipovy Log rare metal pegmatite, central Urals. Russia. Miner Depos. 38, 251–257.
Mao, J.W., Wang, Y.T., Li, H.M., Pirajno, F., Zhang, C.Q., Wang, R.T., 2008. The relationship of mantle–derived fluids to gold metallogenesis in the Jiaodong Peninsula: evidence from D-O–C–S isotope systematics. Ore Geol. Rev. 33, 361–381.
Menzies, M.A., Fan, W.M., Zhang, M., 1993. Palaeozoic and Cenozoic lithoprobes and the loss of >120 km of Archean lithosphere, Sino-Korean craton. China. Geol. Soc. Lond. Spec. Publ. 76, 71–81.
Mills, S.E., Tomkins, A.G., Weinberg, R.F., Fan, H.R., 2015. Anomalously silver–rich vein–hosted mineralisation in disseminated–style gold deposits, Jiaodong gold district. China. Ore Geol Rev. 68, 127–141.
Nie, F.J., Jiang, S.H., Liu, Y., 2004. Intrusion-Related Gold Deposits of North China Craton, People's Republic of China. Resour Geol 54, 299–324.
Qiu, Y.M., Groves, D.I., McNaughton, N.J., Wang, L.G., Zhou, T.H., 2002. Nature, age, and tectonic setting of granitoid–hosted, orogenic gold deposits of the Jiaodong Peninsula, eastern North China Craton. China. Miner Depos. 37, 283–305.
Qiu, X.P., Wang, S.H., Zou, Q., 2008. Metallogenetic effect of Tan–Lu fault on gold accumulation area in Shandong Peninsula. China. Anhui Geology. 18, 19.
Rasmussen, B., Stephen, S., Ian, R.F., 2006. Testing ore deposit models using in situ U-Pb geochronology of hydrothermal monazite: Paleoproterozoic gold mineralization in northern Australia. Geology 34, 77–80.
Selby, D., Creaser, R.A., 2001. Re-Os geochronology and systematics in molybdenite from the Endako porphyry molybdenum deposit. British Columbia. Canada. Econ Geol. 96, 197–204.
Selby, D., Creaser, R.A., 2004. Macroscale NTIMS and microscale LA–MC–ICP–MS Re–Os isotopic analysis of molybdenite: Testing spatial restrictions for reliable Re–Os age determinations, and implications for the decoupling of Re and Os within molybdenite. Geochim. Cosmochim. Acta 68, 3897–3908.
Seo, J.H., Guillong, M., Heinrich, C.A., 2012. Separation of molybdenum and copper in porphyry deposits: The roles of sulfur, redox, and pH in ore mineral deposition at Bingham Canyon. Econ Geol. 107, 333–356.
Smith, H.A., Giletti, B.J., 1997. Lead diffusion in monazite. Geochim. Cosmochim. Acta 61, 1047–1055.
Smoliar, M.I., Walker, R.J., Morgan, J.W., 1996. Re–Os ages of group IIA, IIIA, IVA, and IVB iron meteorites. Science 271, 1099–1102.
Snee, L.W., Sutter, J.F., Kelly, W.C., 1988. Thermochronology of economic mineral deposits; dating the stages of mineralization at Panasqueira, Portugal, by high-precision $^{40}Ar/^{39}Ar$ age spectrum techniques on muscovite. Econ Geol. 83, 335–354.
Song, M.C., Li, S.Z., Santosh, M., Zhao, S.J., Yu, S., Yi, P.H., Cui, S.X., Lv, G.X., Xu, J.X., Song, Y.X., Zhou, M.L., 2015. Types, characteristics and metallogenesis of gold deposits in the Jiaodong Peninsula, Eastern North China Craton. Ore Geol Rev. 65, 612–625.
Stein, H.J., Sundblad, K., Markey, R.J., Morgan, J.W., Motuza, G., 1998. Re–Os ages for Archean molybdenite and pyrite, Kuittila-Kivisuo, Finland and Proterozoic molybdenite, Kabeliai, Lithuania: testing the chronometer in a metamorphic and metasomatic setting. Miner Depos. 33, 329–345.
Stein, H.J., Markey, R.J., Morgan, J.W., Hannah, J.L., Scherstén, A., 2001. The remarkable Re–Os chronometer in molybdenite: how and why it works. Terra Nova 13, 479–486.
Sun, F.Y., Shi, Z.L., Feng, B.Z., 1995. The Geology of Gold Deposits in Jiaodong and the Petrogenesis and Metallogenesis of Mantle-Derived CHO Fluids. People's Publishing House of Jilin, Changchun, p. 170.
Sun, J.F., Yang, J.H., Wu, F.Y., Xie, L.W., Yang, Y.H., Liu, Z.C., Li, X.H., 2012. In situ U-Pb dating of titanite by LA–ICPMS. Chinese Sci Bull. 57, 2506–2516.
Suzuki, K., Adachi, M., 1994. Middle Precambrian detrital monazite and zircon from the Hida gneiss on Oki-Dogo Island, Japan: their origin and implications for the correlation of basement gneiss of Southwest Japan and Korea. Tectonophysics 235, 277–292.
Tan, J., Wei, J.H., Audétat, A., Pettke, T., 2012. Source of metals in the Guocheng gold deposit, Jiaodong Peninsula, North China Craton: link to early Cretaceous mafic magmatism originating from Paleoproterozoic metasomatized lithospheric mantle. Ore Geol. Rev. 48, 70–87.
Tang, J., Zheng, Y.F., Wu, Y.B., Gong, B., Zha, X., Liu, X., 2008. Zircon U-Pb age and geochemical constraints on the tectonic affinity of the Jiaodong terrane in the Sulu orogen. China. Precambr Res. 161, 389–418.
Tartese, R., Ruffet, G., Poujol, M., Boulvais, P., Ireland, T.R., 2011. Simultaneous resetting of the muscovite K-Ar and monazite U–Pb geochronometers: a story of fluids. Terra Nova 23, 390–398.
Taylor, R.D., Goldfarb, R.J., Monecke, T., Fletcher, I.R., Cosca, M.A., Kelly, N.M., 2015. Application of U-Th–Pb Phosphate Geochronology to Young Orogenic Gold Deposits: New Age Constraints on the Formation of the Grass Valley Gold District, Sierra Nevada Foothills Province. California. Econ Geol. 110, 1313–1337.
Tera, F., Wasserburg, G.J., 1972. U-Th-Pb systematics in three Apollo 14 basalts and the problem of initial Pb in lunar rocks. Earth and Planetary Sci Lett. 14, 281–304.
Turner, G., Burnard, P., Ford, J.L., Gilmour, J.D., Lyon, I.C., Stuart, F.M., 1993. Tracing fluid sources and interactions. Philos. Trans. R. Soc. Lond. Ser. A: Math. Phys. Eng. Ser. 344, 127–140.
Voudouris, P.C., Melfos, V., Spry, P.G., Bindi, L., Kartal, T., Arikas, K., Moritz, R., Ortelli, M., 2009. Rhenium-rich molybdenite and rheniite in the Pagoni Rachi Mo–Cu–Te–Ag–Au prospect, northern Greece: implications for the Re geochemistry of porphyry-style Cu–Mo and Mo mineralization. Can Mineral. 47, 1013–1036.
Wang, L.G., Qiu, Y.M., McNaughton, N.J., Groves, D.I., Luo, Z.K., Huang, J.Z., Miao, L.C., Liu, Y.K., 1998. Constraints on crustal evolution and gold metallogeny in the northeastern Jiaodong Peninsula, China, from SHRIMP U-Pb zircon studies of granitoids. Ore Geol. Rev. 13, 275–291.
Wen, B.J., Fan, H.R., Santosh, M., Hu, F.F., Pirajno, F., Yang, K.F., 2015a. Genesis of two different types of gold mineralization in the Linglong gold field, China: Constrains from geology, fluid inclusions and stable isotope. Ore Geol Rev. 65, 643–658.
Wen, B.J., Fan, H.R., Hu, F.F., Yang, K.F., Liu, X., Cai, Y.C., Sun, Z.F., Sun, Z.F., 2015b. The genesis of pegmatite type molybdenum mineralization in Sanshandao, and their implications for molybdenum deposit in Jiaodong. East China. Acta Petrol Sin. 31, 1002–1014.
Wiedenbeck, M., Alle, P., Corfu, F., Griffin, W.L., Meier, M., Oberli, F., Quadt, A.V., Roddick, J.C., Spiegel, W., 1995. Three natural zircon standards for U-Th–Pb, Lu–Hf, trace element and REE analyses. Geostandards Geoanal Res. 19, 1–23.
Wu, F.Y., Yang, J.H., Wilde, S.A., Zhang, X.O., 2005. Geochronology, petrogenesis and tectonic implications of Jurassic granites in the Liaodong Peninsula. NE China. Chem Geol. 221, 127–156.
Wu, M., Zhao, G., Sun, M., Li, S., He, Y., Bao, Z., 2013. Zircon U-Pb geochronology and Hf isotopes of major lithologies from the Yishui Terrane: implications for the crustal evolution of the Eastern Block, North China Craton. Lithos 170–171, 164–178.
Wu, M., Zhao, G., Sun, M., Bao, Z., Tam, P.Y., He, Y., 2014. Tectonic affinity and reworking of the Archaean Jiaodong Terrane in the Eastern Block of the North China Craton: evidence from LA-ICP-MS U-Pb zircon ages. Geol Mag. 151, 365–371.
Xiao, B., Li, Q., Liu, S., Wang, Z., Yang, P., Chen, J., Xu, X., 2014. Highly fractionated Late Triassic I–type granites and related molybdenum mineralization in the Qinling orogenic belt: geochemical and U-Pb–Hf and Re–Os isotope constraints. Ore Geol Rev. 56, 220–233.
Xie, L.W., Zhang, Y.B., Zhang, H.H., Sun, J.F., Wu, F.Y., 2008. In situ simultaneous determination of trace elements, U-Pb and Lu-Hf isotopes in zircon and baddeleyite. Chinese Sci Bull. 53, 1565–1573.
Xie, Z.P., Keiko, H., Jian, W., 2013. Origins of ultramafic rocks in the Sulu Ultrahigh-pressure Terrane, Eastern China. Lithos 178, 158–170.
Xu, P., Zhao, D., 2009. Upper-mantle velocity structure beneath the North China Craton: implications for lithospheric thinning. Geophys J Int. 177, 1279–1283.
Xu, J.W., Zhu, G., Tong, W.X., Cui, K.R., Liu, Q., 1987. Formation and evolution of the Tancheng-Lujiang wrench fault system: a major shear system to the northwest of the Pacific Ocean. Tectonophysics 134, 273–310.
Xu, K.Q., Lu, J.J., Ni, P., 1992. The petrochemical and geochemical characteristics of the granitoids associated with gold deposits. J. Guiling Inst. Metall. Geol. 1, 1–11 (in Chinese with English abstract).
Xu, Y.Q., Lv, G.X., Wang, K., 2013. Detachment fault alteration zone and its fluid mineralization characteristics of the XiaDian gold deposit. Jiaodong province. Acta Mineral Sin. S2, 977–978 (in Chinese).
Yang, W., Li, S.G., 2008. Geochronology and geochemistry of the Mesozoic volcanic rocks in Western Liaoning: implications for lithospheric thinning of the North China Craton. Lithos, 88–117.
Yang, J.H., Zhou, X.H., 2001. Rb–Sr, Sm–Nd, and Pb isotope systematics of pyrite: implications for the age and genesis of lode gold deposits. Geol. 29, 711–714.
Yang, J.H., Wu, F.Y., Wilde, S.A., 2003. A review of the geodynamic setting of large-scale late Mesozoic gold mineralization in the North China Craton: an association with lithospheric thinning. Ore Geol. Rev. 23, 123–152.
Yang, J.H., Chung, S.L., Wilde, S.A., Wu, F.Y., Chu, M.F., Lo, C.H., Fan, H.R., 2005. Petrogenesis of post–orogenic syenites in the Sulu orogenic belt, East China: geochronological, geochemical and Nd–Sr isotopic evidence. Chem. Geol. 214, 99–125.
Yang, J.H., Wu, F.Y., Wilde, S.A., Liu, X.M., 2007. Petrogenesis of Late Triassic granitoids and their enclaves with implications for post–collisional lithospheric thinning of the Liaodong Peninsula. North China Craton. Chem Geol. 242, 155–175.
Yang, J., Gao, S., Chen, C., Tang, Y., Yuan, H., Gong, H., Xie, S., Wang, J., 2009. Episodic crustal growth of North China as revealed by U-Pb age and Hf isotopes of detrital zircons from modern rivers. Geochim. Cosmochim. Acta 73, 2660–2673.
Yang, K.F., Fan, H.R., Santosh, M., Hu, F.F., Wilde, S.A., Lan, T.G., Lu, L.N., Liu, Y.S., 2012. Reactivation of the Archean lower crust: implications for zircon geochronology, elemental and Sr–Nd–Hf isotopic geochemistry of late Mesozoic granitoids from northwestern Jiaodong Terrane, the North China Craton. Lithos 146, 112–127.

Yang, Q.Y., Santosh, M., Shen, J.F., Li, S.R., 2013. Juvenile vs. recycled crust in NE China: Zircon U-Pb geochronology, Hf isotope and an integrated model for Mesozoic gold mineralization in the Jiaodong Peninsula. Gondwana Res. 25, 1445–1468.

Yang, L.Q., Deng, J., Goldfarb, R.J., Zhang, J., Gao, B.F., Wang, Z.L., 2014. $^{40}Ar/^{39}Ar$ geochronological constraints on the formation of the Dayingezhuang gold deposit: New implications for timing and duration of hydrothermal activity in the Jiaodong gold province. China. Gondwana Res. 25, 1469–1483.

Yang, L.Q., Deng, J., Wang, Z.L., Zhang, L., Goldfarb, R.J., Yuan, W.M., Weinberg, R.F., Zhang, R.Z., 2016. Thermochronologic constraints on evolution of the Linglong Metamorphic Core Complex and implications for gold mineralization: A case study from the Xiadian gold deposit, Jiaodong Peninsula, eastern China. Ore Geol. Rev. 72, 165–178.

York, D., 1969. Least-squares fitting of a straight line with correlated errors. Earth Planet Sci Lett. 5, 320–324.

Zhai, M.G., Yang, J.H., Liu, W.J., 2001. Large clusters of gold deposits and large–scale metallogenesis in the Jiaodong Peninsula of Eastern China. Sci. China Ser D. 44, 758–768.

Zhang, Z.H., Zhang, J.X., Ye, S.Z., 1994. The Isotopic Age of Gold Deposits in Jiaodong Peninsula, vol. 1. Seismology Press, Beijing, pp. 9-28.

Zhang, L.C., Shen, Y.C., Li, H.M., Zeng, Q.D., Li, G.M., Liu, T.B., 2002. Helium and argon isotopic compositions of fluid inclusions and tracing to the source of ore-forming fluids for Jiaodong gold deposits. Acta Petrologica Sinica 18, 559–565.

Zhang, L.C., Shen, Y.C., Liu, T.B., Zeng, Q.D., Li, G.M., Li, H.M., 2003. $^{40}Ar/^{39}Ar$ and Rb-Sr isochron dating of the gold deposits on northern margin of the Jiaolai Basin, Shandong, China. Sci. China, Ser. D Earth Sci. 46, 708–718.

Zhang, H.Y., Hou, Q.L., Cao, D.Y., 2006. Study on Mesozoic thrust and nappe tectonics in Eastern Jiaodong. Science in China Series D: Earth Sci. 36, 497–506 (in Chinese).

Zhang, J., Zhao, Z.F., Zheng, Y.F., Liu, X., Xie, L., 2012. Zircon Hf–O isotope and whole-rock geochemical constraints on origin of postcollisional mafic to felsic dykes in the Sulu orogen. Lithos 136, 225–245.

Zhou, T.H., Lü, G.X., 2000. Tectonics, granitoids and mesozoic gold deposits in East Shandong. China. Ore Geol. Rev. 16, 71–90.

Zhou, X.H., Yang, J.H., Zhang, L.C., 2003. Metallogenesis of superlarge gold deposits in Jiaodong region and deep processes of subcontinental lithosphere beneath North China Craton in Mesozoic. Science in China, Serials D 46 (supplement), 14–25.

Zhu, G., Niu, M.L., Xie, C.L., Wang, Y.S., 2010. Sinistral to normal faulting along the Tan–Lu Fault zone: evidence for geodynamic switching of the east China continental margin. J Geol. 118, 277–293.

Zhu, G., Jiang, D., Zhang, B., Chen, Y., 2012. Destruction of the eastern North China Craton in a backarc setting: Evidence from crustal deformation kinematics. Gondwana Res. 22, 86–103.

Zhu, R.X., Fan, H.R., Li, J.W., Meng, Q.R., Li, S.R., Zeng, Q.D., 2015. Decratonic gold deposits. Sci. China: Earth Sci. 58, 1523–1537.